Coordination Chemistry Reviews 253 (2009) 1833–1853

Contents lists available at ScienceDirect

Coordination Chemistry Reviews

journal homepage: www.elsevier.com/locate/ccr

Review

Photonic interfacial supramolecular assemblies incorporating transition metals

Robert J. Forster*, Tia E. Keyes

School of Chemical Sciences, National Bioimaging Platform, National Centre for Sensor Research, Dublin City University, Glasnevin, Dublin 9, Ireland

Contents

ARTICLE INFO

Article history:
Received 18 June 2008
Accepted 9 February 2009
Available online 21 February 2009

Keywords:
Interface
Monolayer, multilayer, photonic, optoelectronic, transition metal
Molecular array

ABSTRACT

The fabrication of nanoscale photonic and electronic devices will rely heavily on bottom up approaches for producing highly organized functional materials. These approaches offer distinct advantages over conventional lithography especially in terms of the spatial precision with which such structures can be built. One of the key barriers to producing operational devices is that of connectivity between the nanoscale and macroscopic world. Interfacial supramolecular chemistry provides this connectivity by combining writeable/addressable surfaces with functional materials. Tremendous progress has been made in the area of interfacial assembly over the past decade. The chemistry for creation of mono- and multilayer assemblies is now well established and increasingly, photoaddressability is being incorporated into such films. Coordination compounds are valuable components in interfacial photonic arrays because they can be "programmed" to perform multiple functions such as surface immobilization, electron transfer and

* Corresponding author. Tel.: +353 170 05943.
E-mail address: robert.forster@dcu.ie (R.J. Forster).

0010-8545/$ – see front matter
doi:10.1016/j.ccr.2009.02.009

light emission with relative synthetic ease. In particular, coordination compounds, e.g., osmium, ruthenium, rhodium polypyridyl complexes, are attractive as their optical transitions are usually well defined, and in the case of charge transfers, strongly allowed, typically occurring in the visible spectral region. Their luminescence can be used as a probe of the interfacial environment or for creating light addressable functionality within a film. Also, they frequently exhibit reversible electrochemical responses across a number of different oxidation states. Although exploitation of such coordination compounds is not as extensive as organic fluorphores, the number of photoactive interfacial films, incorporating photochemically active coordination compounds is growing significantly. Here, we review some key examples, focusing on how coordination compounds can be exploited to drive layer formation and photophysical and photochemical events at interfaces.

1. Introduction and scope

Photonics underpins many of the significant technological advances of the past 50 years. For example, the advent of laser technology and development of optical media have revolutionized the way we store and retrieve information. The prevalence of optical devices is set to continue and further miniaturization demands that well-defined light addressable molecular systems are developed for integration into circuitry or devices. Moreover, the increasing interest in developing efficient solar energy technologies requires molecular arrays to be engineered with exquisite thermodynamic and spatial control of the reagents. This requires deeper insights into the mechanisms of optically driven processes from surface immobilized luminophores. The photon offers an important route to addressability and represents an important strategy for overcoming the "interconnect" problem between the nanoscopic and macroscopic worlds. However, the photonic properties of the adsorbed species will frequently be influenced by the solid substrate and an understanding of the properties and functioning of the assembly rather than the discrete building blocks is essential.

Surface active transition metal complexes are versatile building blocks which are increasingly exploited in interfacial supramolecular assemblies on conducting platforms. The platform influences the opto-electronic properties of the array and provides an in-built electronic interconnect to the macroscopic world. Such interfacial photonic arrays are likely to underpin a diverse range of devices including low cost, high-brightness displays, photovoltaics and sensors capable of detecting disease biomarkers at picomolar concentration.

This article critically reviews key approaches to the construction, characterization and properties of interfacial photonic arrays. In particular, it focuses on those built from coordination compounds of transition metals capable of self-assembling into ordered structures [1–6]. While metal complexes have been widely exploited in redox active arrays, their application in photonic arrays is much less widely developed where the majority of films have relied on organic assemblies [7]. However, in this contribution we discuss self-assembled monolayers (SAMs) and multilayers exploiting transition metal complexes with interesting photonic properties and review recent advances in the theory describing interfacial photophysics. Finally, examples of applications in molecular optoelectronics, sensors and display devices are presented.

1.1. Self-assembled two- and three-dimensional interfacial structures

It is widely recognized that functionally useful thin layers need to self-organize into hierarchical structures as well as form interconnects with the macroscopic world. For many such films based on inorganic or hybrid inorganic–organic compounds, the primary, secondary, tertiary, and quaternary levels of structural organization should ideally be controlled in a manner similar to that achieved in biological systems.

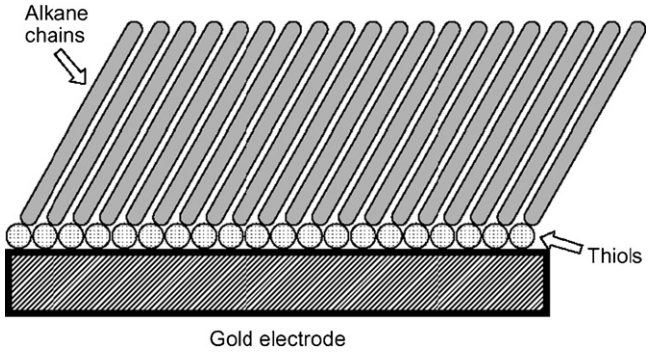

Fig. 1. An organized monolayer on a substrate (electrode). The monolayer can be deposited by the LB method or by self-assembly [8].

1.2. Two-dimensional structures: self-assembled and spontaneously adsorbed monolayers

Spontaneously adsorbed and self-assembled monolayers are similar in that both involve strong binding of a surface active functional group to a surface but are distinct in that a self-assembled monolayer (SAM) also involves stabilizing lateral interactions (secondary structure) between the adsorbates. In this approach, it is possible to create a single layer of molecules on a substrate in which the molecules exhibit significant long-range order through close packing of highly oriented adsorbates. As illustrated in Fig. 1, long-chain thiols and disulfides spontaneously form remarkably well-packed and stable monolayers on gold and other coinage metals [8,9].

1.3. Functional groups for self-assembly

1.3.1. Sulfur anchor-based monolayers

For SAMs formed at metal surfaces, thiols are perhaps the most widely reported surface active functionality. Thiols, R–SH functionality and related molecules, such as disulfides, RS–SR, are particularly attractive as their monolayers can be easily, usually spontaneously, formed on gold and other metals by simply exposing the substrate to the thiol dissolved in solution. A particularly important feature of thiol-based SAMs is the strength of the thiol–metal bond. The high-bond strength, typically of the order of 100 kJ mol^{-1}, means that the functionalized surfaces are stable when in contact with a wide range of solvents, and across a wide range of potentials and temperatures. While annealing to reduce the defect density can be a slow process, disordered monolayers can typically be deposited within a few minutes. Furthermore, monolayer formation does not require anaerobic, anhydrous or vacuum conditions making it attractive for large scale industrial exploitation. The availability of a wide range of ω-terminated thiols, e.g., halide, ether, alcohol, aldehyde, carboxylic acid, amide, ester, amine and nitrile, means that surfaces with a wide range of chemical reactivities and hydrophobicities can be prepared. With this approach ligands with

more than one chelating site, e.g., an N donor site and a thiol, do not have to be used to form metal complexes. This is an advantage, since surface active functional groups such as thiols also have a significant affinity for metal ions leading to complex mixtures during solution phase synthesis. Also, stepwise assembly at the interface allows complex, multiple metal center, systems to be constructed. Equally, the lateral composition of the monolayer can be controlled either by co-adsorbing two or more different thiol containing metal complexes or by using two sequential adsorption steps. The distribution of the two molecules may vary from intimately mixed to completely phase separated.

1.3.2. Nitrogen anchor-based monolayers

The most common nitrogen anchors are based on pyridine or analogues. Pyridine is well known to adsorb strongly onto gold, platinum and other metals, is easily functionalized and is compatible with the synthesis of many metal complexes. For example, dense monolayers of complexes of the type $[M(L–L)_2L_1L_2]^{n+}$ (Fig. 2) have been formed by spontaneous adsorption onto clean platinum, mercury, gold, silver, carbon and copper; L–L is a bidentate N-donor ligand such as functionalized 2,2′-bipyridyl, L_1 is a monodentate organic or inorganic ligand and L_2 is a linear bis-pyridine ligand such as 4,4′-bipyridyl, 1,2-bis-pyridylethane or 4,4′-trimethylene dipyridine [10–13].

Metal substrates have traditionally been an important focus of SAM formation, principally because of their electrochemical addressability. However, the range of substrates has rapidly expanded over the past 10 years and the chemical functionalization of substrates such as glass, and metal or non-metal oxide semiconductors such as TiO_2, fluoride doped tin oxide and indium tin oxide has become commonplace. This diversification has been driven by the need to produce mono- or multilayers on optically transparent materials for display and photovoltaic applications. Organosilicon compounds such as chlorosilanes, alkoxysilanes with long alkyl chains self-assemble on doped metal oxides such as SnO_2, silicon with a thin oxide coating and even gold without any surface oxide. The silyl esters can form SiO_2 linkages with glass and with the oxide layer of silicon. Carboxy functionalities have been extensively used for oxide surface assemblies, most notably with TiO_2. Less common are SAMs based on adsorption of isonitriles which form on metals.

1.4. Solution phase deposition

The dynamics of thiol monolayer assembly have been extensively investigated and these studies reveal that, for deposition solutions containing millimolar concentrations of the thiol, monolayers form within a few seconds. However, these monolayers are highly defective and if left in contact with the deposition solution

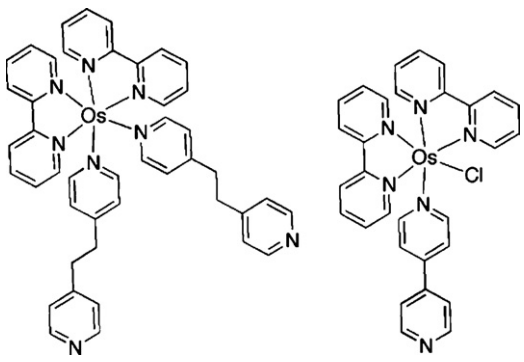

Fig. 2. Surface active osmium polypyridyl complexes used to form spontaneously adsorbed monolayers on metallic electrodes [10–12].

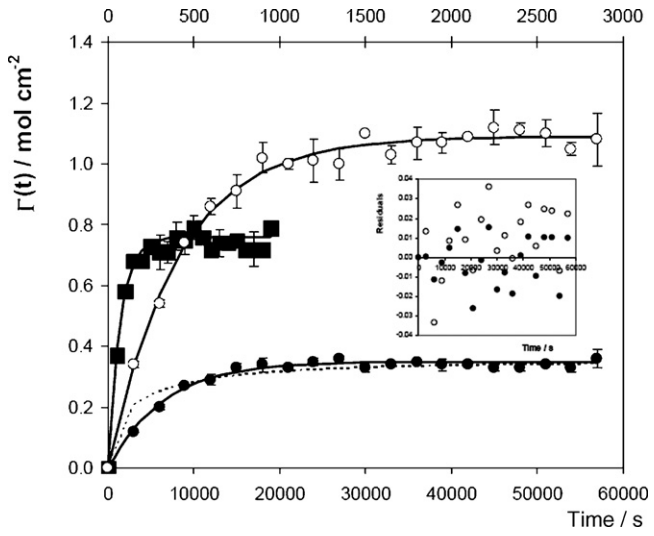

Fig. 3. Temporal evolution in the surface coverage of $[Ru(bpy)_2Qbpy]^{2+}$ adsorbed onto platinum microelectrodes. The bulk concentrations of the complex dissolved in 2:1 H_2O:DMF are 50 μM (□, *x*-axis to the top), 10 μM (■, *x*-axis to bottom) and 1 μM (●, *x*-axis to bottom). For the 1 μM data, the thick solid and dashed lines represent best fits of the first and second order models, respectively. The error bars represent data taken from at least three independent monolayers. The inset illustrates residuals for the first (●) and second order (○) models where the bulk concentration is 1 μM [14].

will slowly anneal over several days to give a low-defect density surface. Detailed spectroscopic studies reveal that the alkane thiols initially adsorb horizontally onto the metal surface followed by reorientation and infilling to give a dense monolayer. On gold, STM studies indicate that monolayer formation is accompanied by etching of the surface and gold has been detected in the deposition solution during self-assembly.

The adsorption dynamics of species capable of forming spontaneously adsorbed monolayers have also been investigated [14]. For example, Fig. 3 shows the change in the surface coverage, Γ with time when the concentration of $[Ru(bpy)_2(Qbpy)_2]^{2+}$ in the deposition solution is 1, 10 or 50 μM, Qbpy is 2,2′:4,4″:4′,4″-quarterpyridyl. For each concentration, Γ initially increases relatively rapidly and then reaches a limiting value at times ranging from approximately 7500 to 20,000 s. Both first and second order models reproduce the general shape of the experimental Γ vs. t profile. However, as illustrated in the inset of Fig. 3, the residuals found for the second order model are larger and are not random with respect to time. This observation, coupled with the fact that the experimental data can be modeled with a concentration independent rate constant, suggests that the more simple, first order model is adequate. The rate constant obtained is $5.1 \pm 0.2 \times 10^{-6}\ s^{-1}$ for $200 < C_B < 1$ μM. The limiting surface coverage is $1.1 \pm 0.1 \times 10^{-10}$ mol cm^{-2} for $20 \leq C_B \leq 100$ μM, i.e., for this range of bulk concentrations dense monolayer coverage is obtained at long times.

1.5. Extending the structure

Extending the dimensionality of SAMs to longer monolayers or to multilayers has chiefly been achieved through two approaches. First, through post-assembly chemical reactions, where reactive groups terminate the SAM and surface-initiated chemical reactions lead to functionalization or graft polymerization on SAM interfaces or through layer-by-layer multilayer self-assembly. This latter approach is most commonly driven by electrostatics but may also be driven by other non-covalent interactions such as inclusion.

1.5.1. Post-deposition modification

The diversity of functional groups that can be used to terminate a SAM forming thiol allows their properties to be tailored for specific applications, e.g., to bind a luminophore after SAM formation. Significantly, this approach often circumvents the difficulty of forming a low-defect density monolayer with structurally complex molecules since assembly proceeds in a stepwise manner using simple building blocks. It is important to note that the reactivity of these terminal groups may be significantly different from that expected on the basis of solution phase reactions because of the low-dielectric constant of the monolayer and restricted physical access. Covalent attachment of functional groups through the formation of amides and esters via acid chlorides and anhydrides or by using carbodiimide coupling, is the dominant approach to post-assembly chemical modification SAMs. In addition, graft polymerization, where for initiation site is built into a SAM has proven an important approach [15]. These approaches produce stable modifications and are synthetically very flexible.

1.6. Multilayer formation

1.6.1. Electrostatically driven assembly

The most common approach to the deposition of ordered multilayers is the layer-by-layer approach based on electrostatic association that was first described by Decher and co-workers [16,17]. Ultrathin multilayer films are formed by alternate deposition of cationic or anionic compounds. This layer-by-layer molecular self-assembly process exploits electrostatic attraction to produce complex layered structures in which it may be possible to precisely control the layer composition and thickness [18]. As shown in Fig. 4, the initial studies tended to focus on polyelectrolyte materials, because a bound polyion reverses the surface charge on the ionized SAM.

Polyoxometallate complexes are finding increasing application in electrostatically assembled multilayer structures because of their large anionic charge, structural diversity, redox activity and capacity for photocatalysis. Anson and co-workers have exploited the strong electrostatic binding properties of heteropolyanions, HPAs, to create heterostructures in which a layer of a multiply-charged heteropolyanion, $[P_2Mo_{18}O_{62}]^{6-}$, was adsorbed irreversibly on the surface of a variety of electrodes and used to bind cations such as $[Os(bpy)_3]^{2+}$ to the surface. Significantly, these investigations reveal that stable multiple layers could be grown by exposing the electrode surface repeatedly to a solution of the heteropolyanion and subsequently to a solution of the $[Os(bpy)^3]^{2+}$ cation [19].

Layer-by-layer electrostatic assemblies of polyoxometalates have also been used for electrochromic display [20] and in sensing applications. For example, Kurth et al. reported on an amperometric sensor for NO based on a multilayer assembly of a polyelectrolyte and a redox active polyoxometalate [21]. The composite multilayer schematically illustrated in Fig. 5 comprises a cobalt(II)-substituted sandwich complex, $[Co(II)_4(H_2O)_2P_4W_{30}O_{112}]^{16-}$ layered with poly(styrenesulfonate) (PSS) and/or poly(allylamine hydrochloride) (PAH). The Co-POM sensitizes the ITO electrode surface toward electrocatalytic reduction of NO from solution. Selectivity toward NO was achieved by adapting the permeability of the film through the architecture of the topmost layers of the film.

Tailoring of nanostructured photoelectrochemical systems is another challenging facet of molecular optoelectronics. Willner has described the construction of layered arrays consisting of nanoparticles cross-linked by molecular functionalities. The cooperative effects in these photoactive molecular cross-linked nanoparticle arrays leads to unique photoelectrochemical properties. For example, as shown in Fig. 6, an initial layer of citrate stabilized Au-nanoparticles on an aminosiloxane-functionalized ITO-electrode can be formed that is then cross-linked by the stepwise association of positively charged photosensitizer–electron acceptor dyads, e.g., the Zn(II)-protoporphyrin IX-bis-bipyridinium, or Ru(II)-*tris*-bipyridine-bis-phenylene (paraquat)-catenane. The photocurrent spectra match the absorption spectrum of the Zn(II)-porphyrin chromophore and the photocurrent is blocked upon biasing the electrode potentials at values that are more negative than the redox potential of the bipyridinium units. This result suggests that the photocurrent originates from the intramolecular electron-transfer quenching of the chromophore by the bipyridinium units, followed by the tunneling of the electrons to the electrode by the conductive array of Au-nanoparticles.

Alternative approaches for non-covalent multilayer assembly exist, e.g., multilayers can be constructed on SAMs via sequential deposition of a metal cation and then a difunctional molecule. Similar coordination chemistry approaches to multilayer formation have also been described. For example, Rubinstein and co-workers described branched coordination multilayers in which molecular-scale control over the film thickness and a high degree

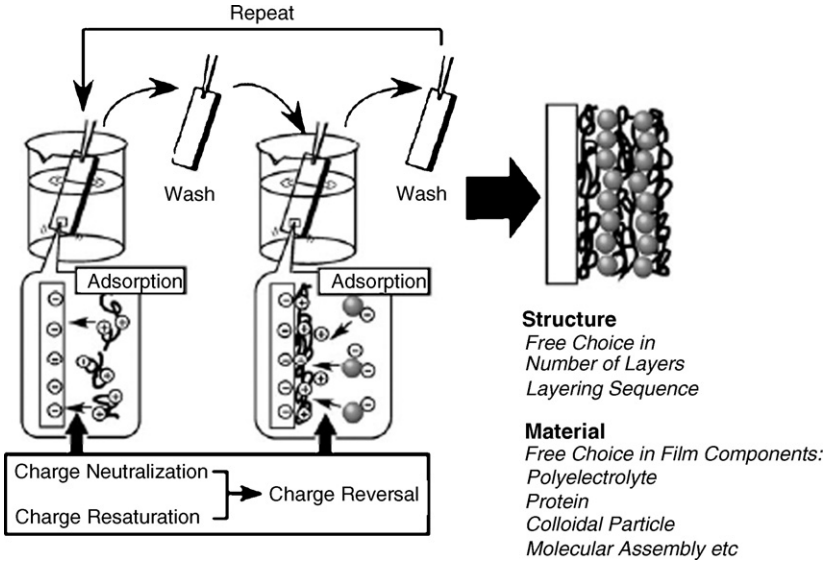

Fig. 4. Schematic outlining layer-by-layer assembly method.

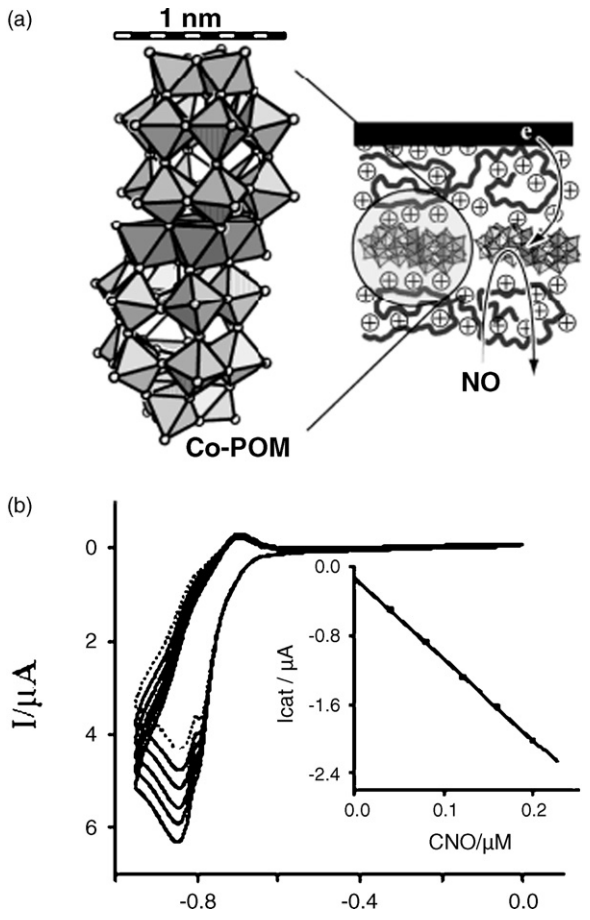

Fig. 5. (a) Schematic representation of POM-based NO sensor. The Co-POM structure comprises four Co centers coordinated through two trivalent Dawson fragments. (b) Cyclic voltammograms of an ITO electrode modified with $(PSS/PAH/Co\text{-}POM/PAH)_3$ at various concentrations of NO: 0, 40, 80, 120, 160, and 200 nM (from top to bottom). Inset: calibration curve corresponding to the electrochemical sensing of NO by the analysis of the second reduction peak of Co-POM anions (all curves are recorded under Ar atmosphere in 0.2 M buffer solution, pH 7.0, scan rate 10 mV s^{-1}) [21].

of homogeneity was achieved [22]. Fig. 7 illustrates the functionalization of gold island films deposited on glass with a disulfide terminated SAM of bis-hydroxamate. Alternate binding of layers of a tridentate hexahydroxamate molecule with C_3 symmetry consisting of three bis-hydroxamate ion-binding sites and Zr^{4+} ions, produced novel coordination multilayers.

As illustrated in Fig. 8, Kurth et al. described layer-by-layer electrostatic assembly of cationic polymer films in which 2,2-bipyridine units were built into the polymer structure to provide coordination sites for metal complexes [23]. Anionic poly(styrene sulfonate) could then be electrostatically bound to the polycationic surface. Metal coordination was achieved, either through exposure of the multilayer to metal ion solution or more elegantly through microcontact stamping of transition metal salts. This latter approach could be used to creating patterned coordination complexes throughout the film.

The multilayer structures were studied using X-ray reflection spectroscopy which provided detailed information on film thickness and characteristics of the layer interface and layer thickness and demonstrated that the layers were well ordered. A number of ions were reversibly bound to the layer (binding reversed on exposure to EDTA) including Zn^{2+} which resulted in a luminescent film reminiscent of $[Zn(bpy)_2]^{2+}$.

One of the drawbacks of electrostatic layer-by-layer assembly is that the level of order that can be attained in the multilayer is highly variable. If a highly ordered second monolayer is required, Langmuir–Blodgett techniques can be used. However, the drawback of LB assembly, which is based on non-covalent assembly is the stability of the layers may be poor. The literature on LB film methods is extensive and will not be addressed in this review [24].

1.7. Photonic properties of monolayers

The functioning of a true supramolecular assembly is not dictated simply by the photonic properties of its component building blocks. Rather its overall function is more than the sum of its parts and is intimately linked with the structure, organization and interactions present within the assembly.

Addressability is of primary concern if SAMs and multilayers are to find real world application. As discussed above, two of the key approaches to building addressability into interfacial assemblies have been to incorporate electrochemically or photochemically active components. However, although the behavior of surface immobilized electrochemically active species is well understood, the behavior of photoactive species immobilized at an interface has received considerably less attention. Nonetheless, it is clear that the photophysical properties, e.g., the emission lifetime, of a molecule may change significantly upon surface immobilization. Depending on a range of parameters from the inherent behavior of the molecule itself, e.g., its oxygen sensitivity, the rigidity of the film and substrate parameters such as presence of a surface plasmon, the immobilized luminophore may be more or less emissive than in solution [25].

1.7.1. Photoinduced electron transfer

First, the main photochemically stimulated events that can occur in an interfacial supramolecular system are discussed [26,27]

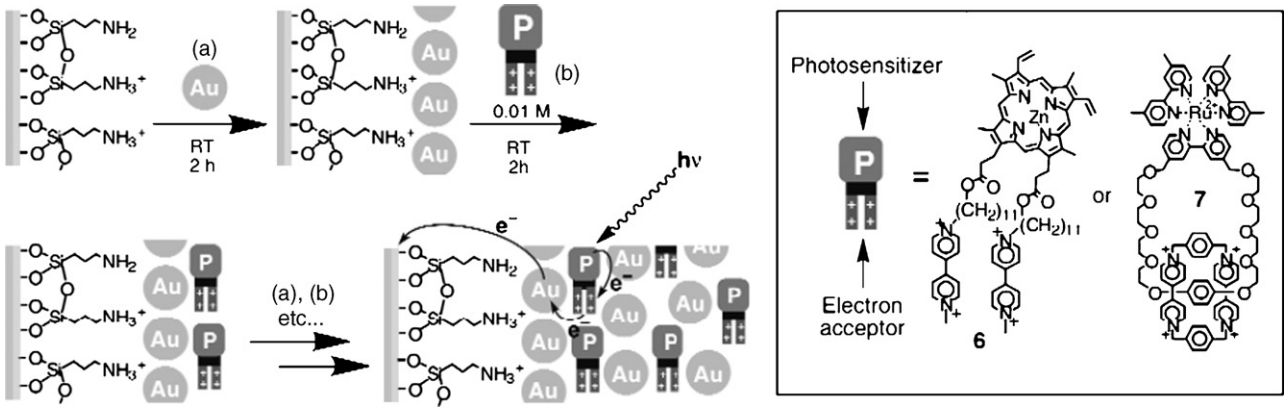

Fig. 6. Assembly of layered photosensitizer–electron acceptor cross-linked Au-nanoparticle arrays on a metal surface for photoelectrochemical applications.

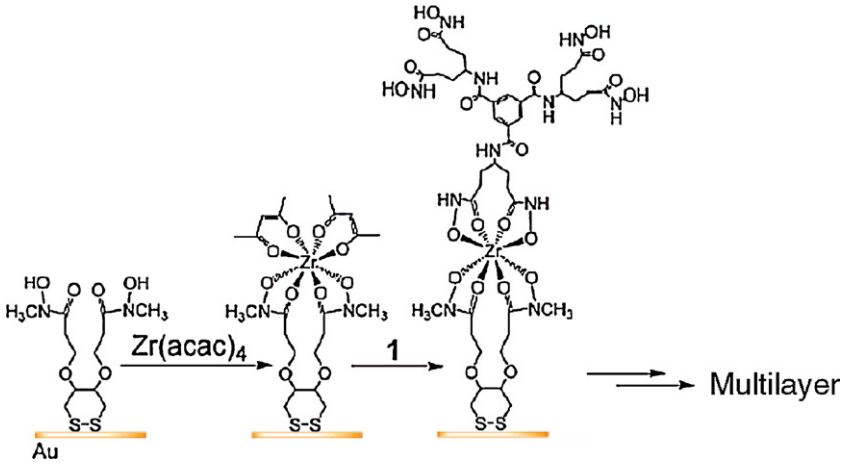

Fig. 7. Multilayer assembly through coordination chemistry. The monolayer provides coordination sites from which the multilayer is built through coordination of transition metals in one or more coordination steps. Here branched coordination multilayers created from SAMs of disulfide terminated of bis-hydroxamate with subsequent coordination of zirconium and hexahydroxamate ligand, created multilayers [22].

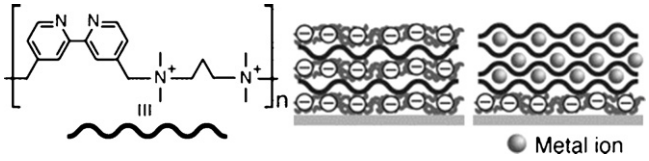

Fig. 8. Schematic of multilayer of bi-functional polyelectrolyte functionalized with bipyridine metal receptor units. Multilayers can be assembled by layer-by-layer assembly with poly(styrene sulfonate), A, or through coordination to metal ions, B [23].

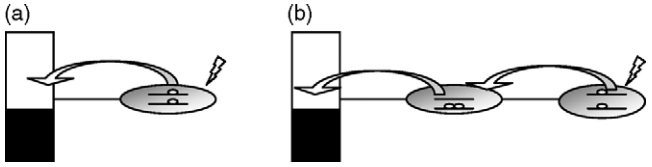

Fig. 9. Schematic showing direct (a) and indirect (b) electron or energy transfer where the photoexcited species injects or accepts an electron directly to or from the electrode.

In photocatalysis and photovoltaics, the adsorbed photoactivated species interacts directly with the metal surface leading to quenching of the excited state. As shown in Fig. 9(a), this process may occur directly whereby the photoexcited species injects or accepts an electron directly to or from the electrode. Alternatively, as shown in Fig. 9(b) photoinjection may be a secondary process following a prior intramolecular electron or energy transfer from another component in the supramolecular assembly. The majority of photoinduced interfacial electron transfers have been conducted at semiconductor substrates, although conductors are increasingly being investigated.

1.7.2. Photoinduced electron transfer at SAMs

One of chemistry's grand challenges remains the construction of a very efficient artificial photoelectric conversion device mimicking natural photosynthesis. Organization, energetics and dynamics all play crucial roles in the successful operation of natural systems. For example, photon absorbers like chlorophyll and electron donors and acceptors like pheophytins and quinones, are highly organized at the molecular length scale to achieve very efficient photoinduced charge separation and electron transfer while minimizing the extent of back reaction [28] Early examples of artificial photosynthetic molecular system using lipid bilayer membranes [29,30] or Langmuir–Blodgett (LB) films [31] function. However,

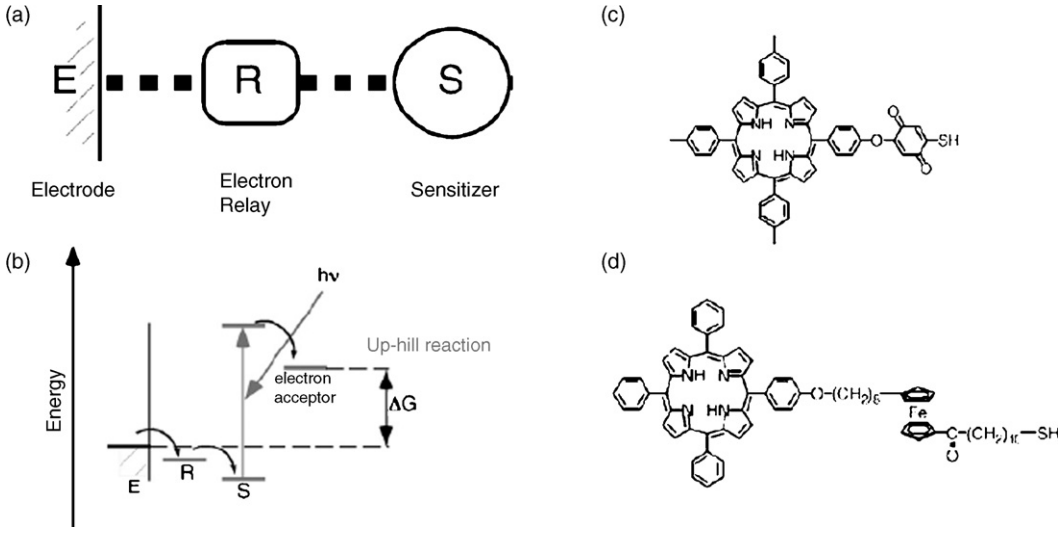

Fig. 10. (a) Molecular scheme of the concept to attain highly efficient photoinduced electron transfer and (b) energy diagram of this system. (c) PQSH molecule and (d) PFcSH molecule [32].

they have low-quantum efficiencies (0.4–1.5%) compared to natural systems because the physical positioning of the components is not sufficiently precise and the thermodynamics and kinetics are not optimal. Alkane thiol-based SAMs have opened up new opportunities in this area allowing highly ordered assemblies to be created. Moreover, issues, such as the distance dependence of electronic coupling between the remote chromophores and the conducting platform can be investigated in significant detail. Fig. 10 illustrates the approach followed by Uosaki et al. [32]. In this approach, the metal electrode is modified with a SAM containing both a photon-absorber and an electron relay within a single surface active molecule. For example, in porphyrin-quinone-thiol (PQSH) or porphyrin-ferrocene-thiol (PFcSH) films the porphyrin acts as the photon absorber and the quinone and ferrocene act as the electron relay group. The extent of lateral interactions can be controlled by incorporating inactive diluent thiols.

When the modified gold electrodes are illuminated with white light in electrolyte solutions containing methylviologen (MV^{2+}) as an electron acceptor, a stable cathodic photocurrent flowed if the electrode potentials were more negative than +200 and +650 mV. This coincides with the redox potentials of the quinone and ferrocene moieties in the SAMs, respectively. Significantly, the photocurrent was stable for periods of several hours and chemical decomposition was not observed. The quantum efficiencies of these systems were more than 3% for the PQSH SAM and more than 10% at the PFcSH SAM. The dependencies of quantum efficiency on the alkyl chain length and the electrode surface roughness revealed that the high efficiency arises from the formation of an ordered SAM that minimizes back electron and energy transfer.

There have been a substantial number of other SAM systems based on coordination compounds for photocurrent generation including the fullerene-porphyrinferrocene-thiol (FuPorFcSH) system illustrated in Fig. 11 created by Imahori et al. [33]. Significantly, such SAMs formed on both gold and indium tin oxide (ITO) exhibit a high-photocurrent efficiency (20–25%) which is thought to arise from the small reorganization energy of the fullerene.

Ishida and Majima demonstrated that excitation of the metal surface plasmon can improve photocurrent generation over that found for conventional direct photoexcitation at a porphyrin-thiol SAM [34]. This observation opens up new opportunities for further efficiency gains by nanostructuring the gold surface.

Depending on the optical properties and extent of quenching by the metallic platform, multilayers may offer advantages over SAMs. The primary layer in these complex assemblies is often a SAM. For example, as illustrated in Fig. 12, Shinkai et al. [35] exploited electrostatic layer-by-layer assembly of a fullerene-cationic homooxacalix[3]arene inclusion complex and anionic porphyrin polymer on an ITO electrode modified with a SAM of

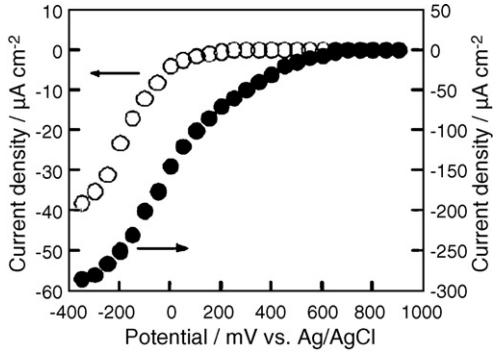

Fig. 11. Potential dependence of photocurrents of PQSH SAM-modified and PFcSH SAM-modified gold electrodes measured in 0.1 M Na_2SO_4 and 0.1 M $NaClO_4$, respectively, containing 5 mM MV^{2+} [33].

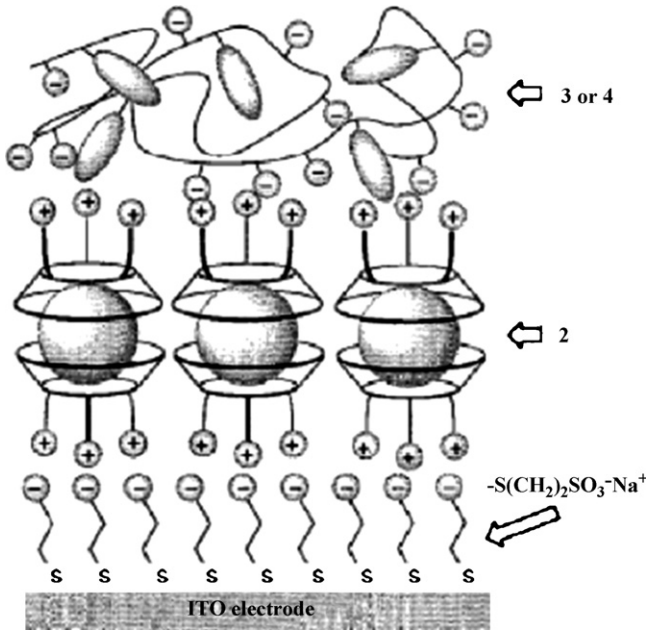

Fig. 12. Schematic view of photoactive multilayers of sodium 3-mercaptoethanesulfonate (first layer), fullerene-cationic homooxacalix[3]arene inclusion complex 2 (second layer), and anionic porphyrin polymer 3 or 4 (third layer) on an ITO electrode [35].

a sulfonate-terminated thiol molecule. These assemblies produce a substantial photocurrent.

Fig. 13 illustrates the electrostatically assembled photoactive multilayers developed by Thompson et al. [36] based on a porphyrin SAM followed by zirconium cation and a phosphate anion.

Many elegant multilayer supramolecular systems for photocurrent generation, including those described above require significant organic synthetic effort. One of the key advantages of coordination chemistry is its relative synthetic simplicity. In many instances, coordination bonds can form spontaneously at room temperature.

Mallouk et al. have pioneered the area of multilayer assembly including the exploitation coordination chemistry in layer-by-layer assembly. Both Mallouk and separately Katz have in particular instigated the development of zirconium phosphonate LBL films which have laid the foundation for a range of elegant interfacial supramolecular structures which have particularly useful in the area of photocatalysis [37,38]. Hoertz and Mallouk recently reviewed the work of Mallouk's group in the area of interfacial photocatalysis [39].

Fig. 14 illustrates multilayer structures built on coordination bonds reported by McGimpsey et al. that produce promising photocurrents [40]. For the coordination multilayers, II and III, decanethiol was linked to a 4-pyridyl-2,6-dicarboxylic acid ligand to for a SAM. This was coordinated to Cu(II) ion and terminated either with a pyridyl-2,6-dicarboxylic acid ligand linked at the 4-position through a methylenyloxy group to a pyrene chromophore or a second coordination was built in, (III), by introducing 4,4′-bipyridyl-2,2′6,6′-tetracarboxylic as a bridging ligand. The photocurrent generation for II and III in which the multilayer is assembled through coordination, is compared with the organic film, I, in the presence of methyl viologen as sacrificial acceptor. A quantum efficiency of approximately 1% was observed from II and III. However, the key advantage of these multilayers compared with I was their considerably enhanced photostability.

While SAMs offer the possibility of high-packing densities, the total number of molecules on the surface is relatively small and extending the array into three-dimensional film may be advantageous. However, the yield of the surface reactions, e.g., electrostatic

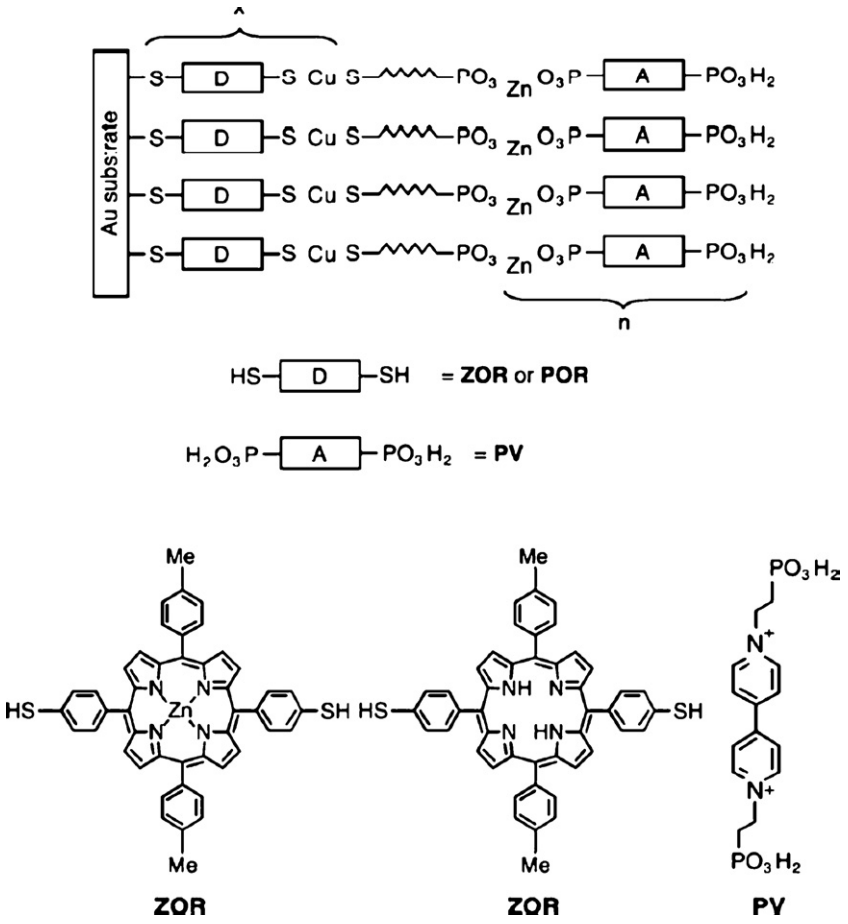

Fig. 13. Schematic of the photoactive multilayers assembled using the porphyrins and viologen derivatives shown [36].

association, host–guest binding or covalent bond formation, that bind successive layers may be low. In contrast, monolayer protected metal nanoparticles and clusters can be conveniently functionalized with thiolated metal complexes using the ligand surface exchange approach developed by Brust and others [41–43]. Alternatively, electrostatic forces can be used to assemble multilayers of anionic citrate stabilized nanoparticles with cationic metal complexes.

While beyond the scope of this review, it is perhaps important to note that semiconducting nanoparticles can also be used in which case not only do the functionalized nanoparticles direct the assembly but the monolayers also dictate the photoelectrochemical properties of the nanoparticles.

Self-assembly approaches have now come of age and can produce hierarchical systems to create useful devices without the need to incorporate nanoscale electrodes to interface to the macroworlds. For example, as illustrated in Fig. 15, Drain [44] has elegantly demonstrated that through careful design of the primary porphyrin building blocks (primary structure), these can self-assemble into supramolecular entities (secondary structure), which are then self-organized into a liquid crystalline matrix (tertiary structure), and form a functioning device (quaternary structure). Specifically, lipid bilayers are used as a means to self-organize the self-assembled porphyrin arrays in terms of both size and orientation. The 1 mm across and 8-nm thick disk-shaped device is then connected to the macroscopic world by using standard laboratory electrodes. Significantly, when the self-assembled photoconductors are illuminated with 100 W of white light and with no applied potential a significant photocurrent is observed. The electrochemical potential between the donor and the acceptor (0.5 V) is the driving force for the photocurrent production.

1.7.3. Light-induced switching and gating

The design and synthesis of functional molecules with molecular switching characteristics is currently an area of intense activity with tremendous potential significance to the fields of molecular electronics and sensors [45]. Molecules, such as azobenzene, that are capable of undergoing photoinduced *cis–trans* isomerization represent an important approach to both switching physical access to the underlying electrode surface and to modulating the extent of electronic communication to a remote chromophore/luminophore/redox couple. For example, as illustrated in Fig. 16, Mirkin and co-workers [46] demonstrated "photon-gating" or "light-switching" of electron transfer at a gold electrode modified with mixed SAMs of FcAzSH and an azobenzene-thiol linked molecule.

Prior to irradiation at 400 nm, the azobenzene-thiol exists in its *cis* form and a catalytic current due to the oxidation of ferrocyanide was observed close to the redox potential of the immobilized ferrocene, showing that mediated electron transfer occurs. Following irradiation at wavelengths longer than 400 nm, the azobenzene switches to its trans configuration and both oxidation and reduction of the ferro/ferricyanide can be observed. Detailed investigations into the electrochemical properties of gold electrodes modified with azobenzenethiol suggest that the redox potential and charge transfer rate of the ferrocene group in the SAM can be reversibly controlled by electro- *and* photochemically triggered conversions between the *cis*- and *trans*-forms of the azobenzene moiety. As illus-

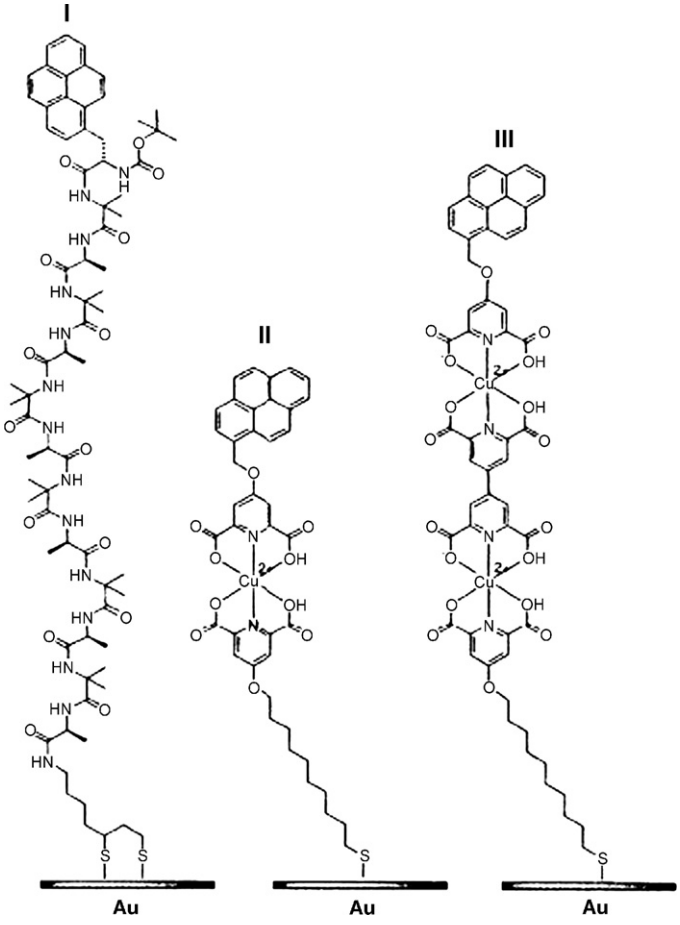

Fig. 14. A coordination multilayer for photocurrent generation [40].

trated in Fig. 17, these processes allow a "pore" to be opened within the monolayer to allow a solution phase species interact directly with the underlying electrode.

An interesting coordination chemistry approach to switching was reported by McGimpsey et al. for a 2,2′-dipyridylethylene ligands in the self-assembled monolayer shown in Fig. 18 [47]. Here, excitation, presumably into the π^* transition of 2,2′-dipyridylethylene, induces a *cis–trans* isomerization which reduces the coordination number of this ligand to Cu(II) in the film resulting in changes to the wettability of the film. The change is however, irreversible which was surprising based on the solution phase chemistry, but serves to highlight how differences in SAM or multilayer photochemistry and solution behavior may arise.

Willner et al. have reported extensively on photoisomerizable monolayers on electrodes, especially those based on spyropyran [48]. For example, as shown in Fig. 19, they exploited the redox chemistry of ferrocene to act as a redox mediator to enhance electrical contact between glucose oxidase (Gox) and the electrode. The nitropyropyran undergoes photoisomerization to its protonated, cationic nitromercyanine form which drives the assembly of the bilayer and initiates electrocatalyzed oxidation of glucose. This process is reversible and by irradiating the assembly with visible light the electrocatalysis can be switched off.

1.7.4. Luminescence from metalloSAMs

Materials that can absorb photons to create an electronically excited state are of particular interest because they are simultaneously better electron donors and acceptors than their ground-state precursors. However, although much is known about the creation and deactivation of electronically excited states in solution, the photophysical behavior of luminophores adjacent to, or immobilized directly on, a metal surface may be complex as there are a large number of possible routes to luminescence quenching or enhancement dictated by the properties of the substrate and the luminophore [49]. In general, if the monolayers are formed on atomically smooth metal surfaces, then excited-state quenching is expected to be efficient if the distance between the excited state and the surface is sufficiently small (<100 Å). Under these circumstances, energy or electron-transfer quenching can occur within the lifetime of the electronically excited state because of the continuum of acceptor states available within the metal. In contrast, when the metal surface is roughened on the nanometer length scale, the luminescence intensity can be enhanced by up to several orders of magnitude due to enhancement of the excitation and/or emitting electromagnetic fields by the surface plasmon of the substrate. Moreover, the emission properties depend on the electrode potential and the redox potentials of the electronically excited state, the structure and length of the bridging ligand, the quantum efficiency for luminescence and the extent of electronic coupling between substrate and luminophore [50,51].

For example, as illustrated in Fig. 20, our group have demonstrated that spontaneously adsorbed monolayers of $[Ru(L–L)_2(Qbpy)]^{2+}$ on platinum microelectrodes leads to emission (L–L is 2,2′-bipyridyl or 4,7-diphenyl-1,10-phenanthroline and Qbpy is 2,2′:4,4″:4′,4″-quarterpyridyl) [52]. While much research has focused on distance as the primary approach to controlling the extent of interaction between the electrode and bound luminophore, these investigations suggest that controlling the structure of the bridging ligand is equally important if near-surface emission is to be achieved.

1.7.5. Direct measurement of the excited-state redox potentials

One of our key interests in these luminescent monolayers has been the *direct* measurement of the excited-state redox potentials. Achieving this goal demands that heterogeneous electron transfer across the electrode/monolayer interface occur on a timescale that is shorter than the luminescent lifetime. Balancing the requirements of fast heterogeneous electron transfer (for which short-electron-transfer distances are optimal) vs. a large distance between metal surface and the excited state to minimize energy-transfer quenching places severe demands on the experimental system.

Conventional electrochemical methods cannot provide a meaningful insight into the redox properties of electronically excited states since traditional voltammetry is restricted to millisecond, or longer, timescales [53]. However, with the advent of ultrafast electrochemical techniques and microelectrodes, it is now possible to directly probe the properties of species having sub-microsecond lifetimes [54]. Fig. 21, illustrates the cyclic voltammetry response observed at a scan rate of 3×10^5 V s^{-1} immediately after photoexcitation of an $[Ru(dpp)_2Qbpy]^{2+}$, where dpp is 4,4′-diphenylphenanthroline with a 10 ns laser pulse at 355 nm [55]. The voltammetric timescale is shorter than the excited-state lifetime and voltammetry characteristic of the electronically excited state can be obtained. This figure shows that on the first scan an oxidative current response is observed at approximately −0.8 V. The peak potential of this process is in approximate agreement with the calculated excited-state redox potential of −0.9 V. That this current response is not observed for the second or subsequent scans confirms the transient nature of the phenomenon.

A complication in the voltammetry shown in Fig. 21 is that the product obtained by oxidizing the electronically excited state is the ground state oxidized product $[Ru(bpy)_2Qbpy]^{3+}$. The complication arises because this ruthenium 3+ species is

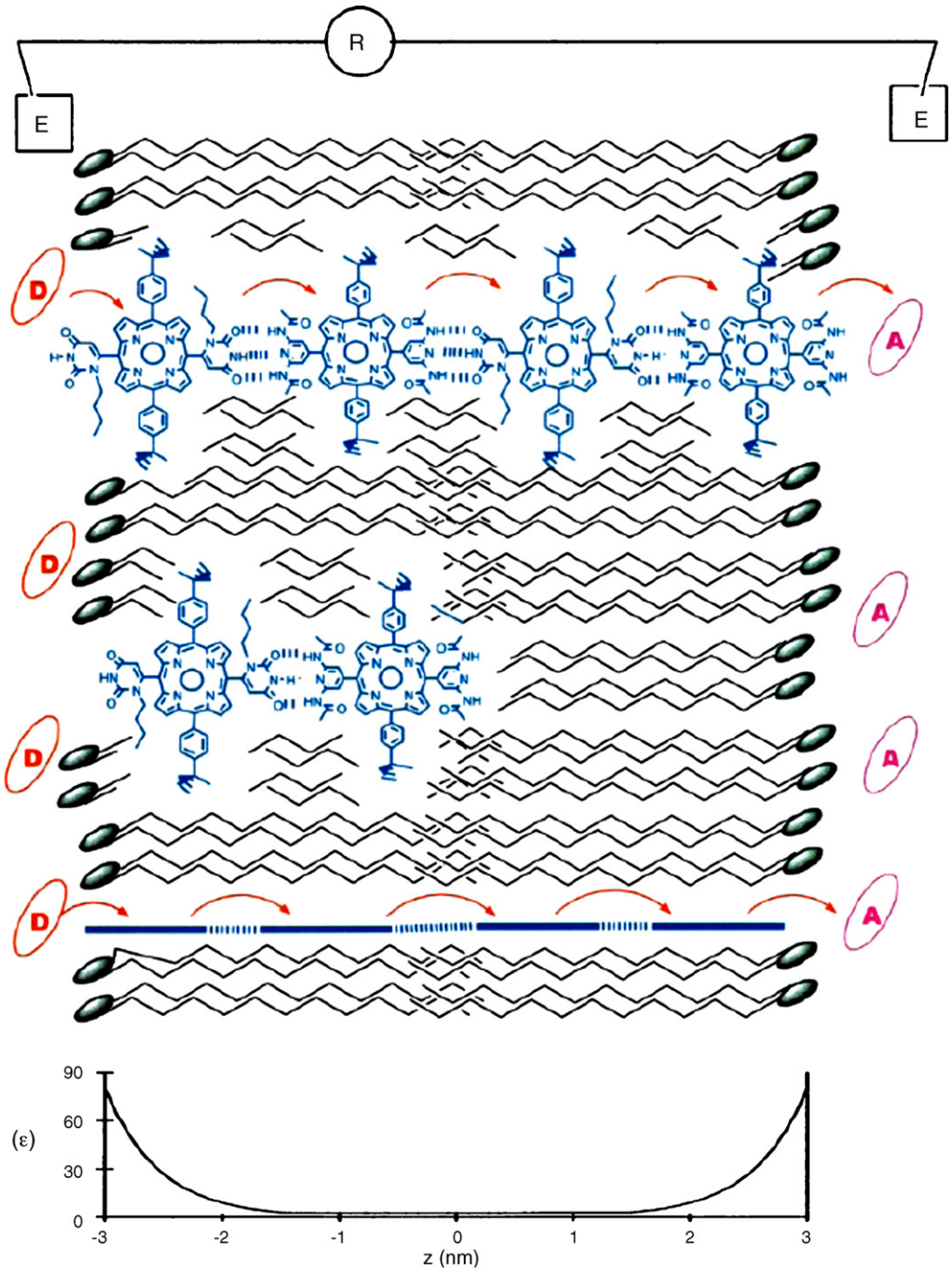

Fig. 15. Schematic of one of four self-assembling porphyrin systems self-organized into bilayers to form a functional device. The orientation of the porphyrin tape (top and bottom arrays) can be in any direction such that the porphyrin planes are perpendicular to the bilayer–water interface. It is difficult to quantify the yield of membrane-spanning porphyrin arrays, so it is reasonable to expect some monomers-to-trimers to be present in the system (middle). The electron donor, D, is $K_4Fe(CN)_6$ and the acceptor, A, is anthraquinonesulfate (AQS). The bottom graph illustrates the exponentially varying dielectric constant [44].

created at a potential that is approximately 1.5 V *negative* of the ground state formal potential. Under these circumstances, one would expect that the ground state product would be rapidly reduced. Thus, as shown in the following scheme, the overall reaction would consist of removal of an electron from the electronically excited species followed by electron injection into the ground state oxidized product, i.e., two opposing electron transfers:

$$[Ru(bpy)_2Qbpy]^{2+*} - e^- \rightarrow [Ru(bpy)_2Qbpy]^{3+}$$ (Irreversible excited state oxidation $E_{peak} \approx -0.8V$)

$$[Ru(bpy)_2Qbpy]^{3+} + e^- \rightarrow [Ru(bpy)_2Qbpy]^{2+}$$ (Irreversible reduction of ground state oxidized product)

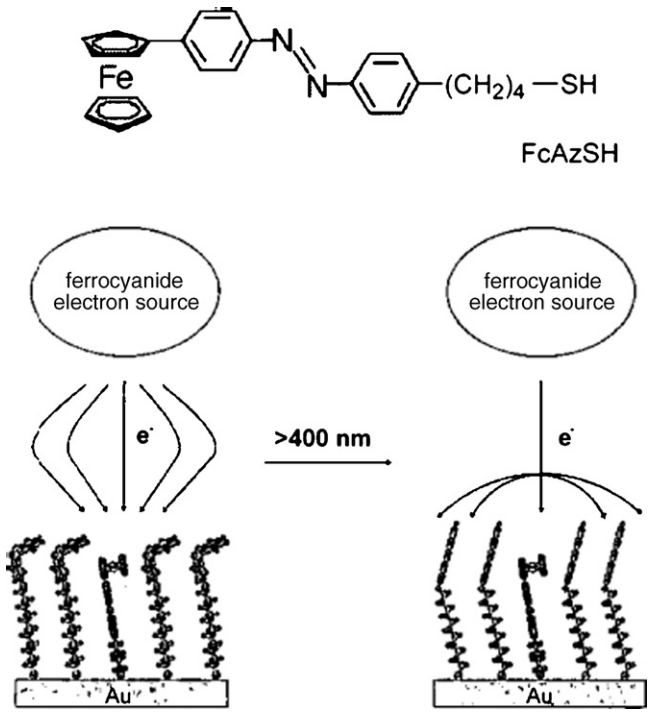

Fig. 16. Schematic illustration of the control of electron transfer by photoirradiation at FcAzSH SAM-modified gold electrodes [46].

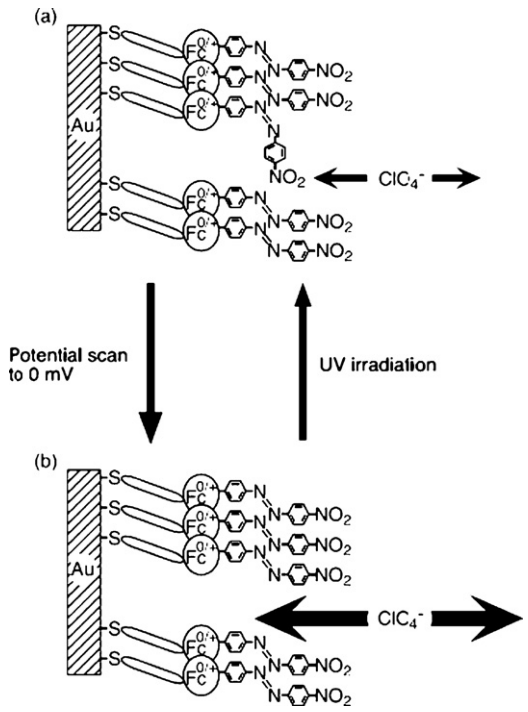

Fig. 17. Schematic illustration at the interface (a) between a 100% *trans*-AzFcSH SAM-modified gold electrode and electrolyte solution containing perchlorate anions and (b) between a 20% *cis*- and 80% *trans*-AzFcSH SAM modified gold electrode and electrolyte solution containing perchlorate anions before the potential scan to 0 mV [46].

Scan rate dependent voltammetry suggests that the relative rates for oxidation of the electronically excited state and the reduction of the ground state product are substantially different.

1.7.6. Lateral quenching

Another feature of luminescent monolayers is that because the surface concentration of the adsorbates can be high (up to six orders of magnitude larger than that used for typical solution phase experiments), lateral energy or electron transfer may lead to quenching of the excited states. Therefore, the ability to control the surface coverage is important. Also, the redox active monolayer can be partially oxidized to create acceptor states, i.e., Ru^{3+}, for photoinduced electron transfer from the electronically excited state, Ru^{2+*}.

Fig. 22 illustrates the effect of electrochemically titrating in defined concentrations of Ru^{3+} into the film on the intensity of the observed emission.

The key feature of Fig. 22 is that the adsorbed $[Ru(dpp)_2Qbpy]^{2+}$ complexes clearly emit despite being only approximately 12 Å above a metal surface. A significant observation is that the monolayer spectrum resembles that observed at 77 K, i.e., the emission maxima and peak shape are similar. This similarity in the spectra suggests that the vibrational degrees of freedom of complexes within the monolayer are significantly reduced.

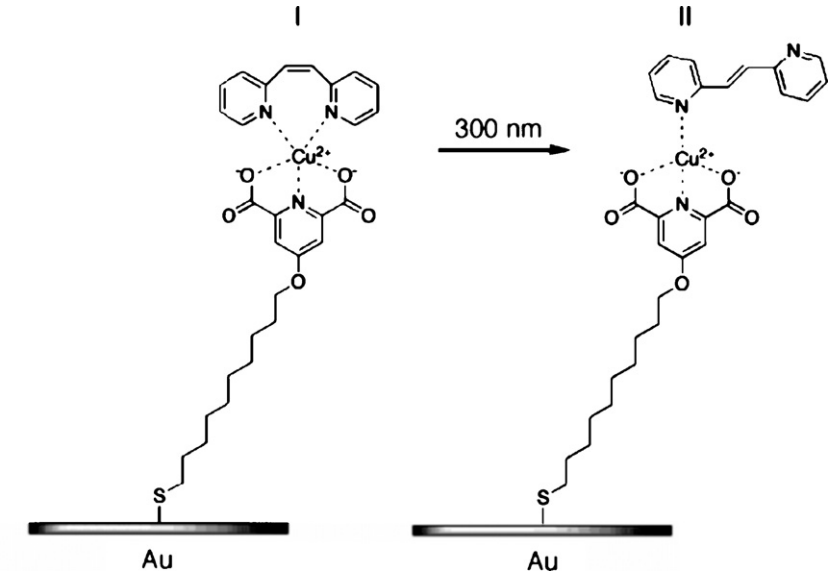

Fig. 18. Photoisomerized coordination change in a self-assembled thiol monolayer [47].

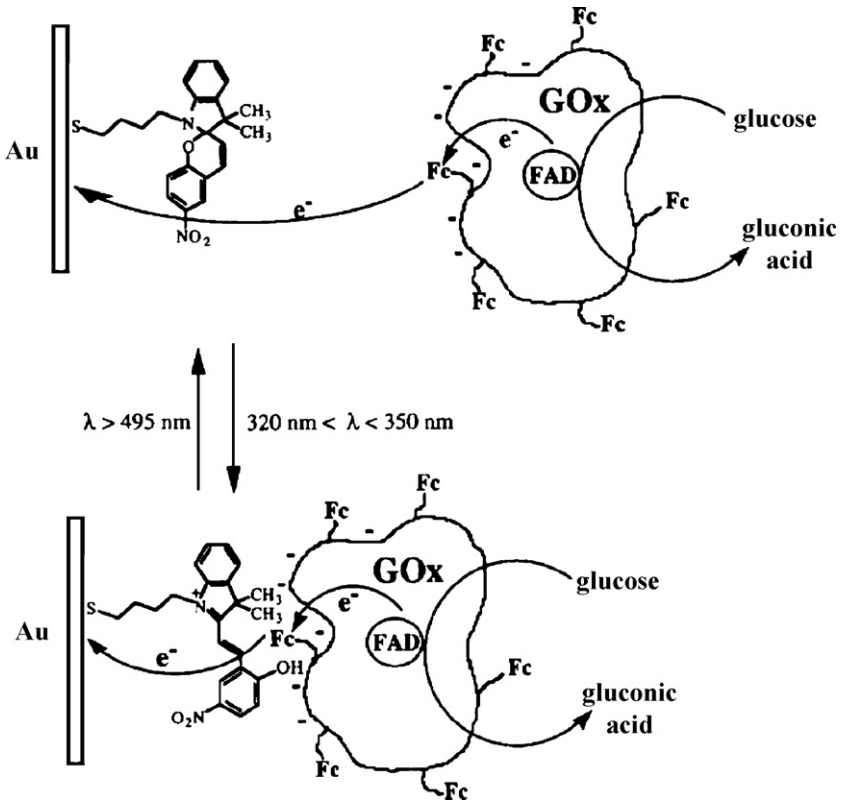

Fig. 19. Electrostatic assembly of ferrocene (Fc) modified glucose oxidase (Gox) on a spyropyran monolayer on gold [48].

To compare the quenching effects observed in these monolayers with previous reports dealing with reactants in solution or within thick films [56–59], the effective three-dimensional concentration of luminophores within the assembly was used. Taking the saturation coverage of 1.1×10^{-10} mol cm^{-2} and the monolayer thickness of approximately 15 Å, the concentration of ruthenium centers is approximately 0.7 M. The quenching response of Fig. 23 can be described by the Stern–Volmer equation:

$$\frac{I_0}{I} = 1 + K_{SV}[Ru^{3+}] \quad (1)$$

where I_0 and I are the fluorescence intensities in the absence and presence of quencher respectively and K_{SV} is the Stern–Volmer constant. It is important to note that because the composition of the film is being controlled electrochemically, some of the loss of luminescence intensity arises because the Ru^{2+} concentration decreases as Ru^{3+} is created. This figure shows that luminescence intensity decays much more rapidly than would be expected on the basis of loss of Ru^{2+*} species alone.

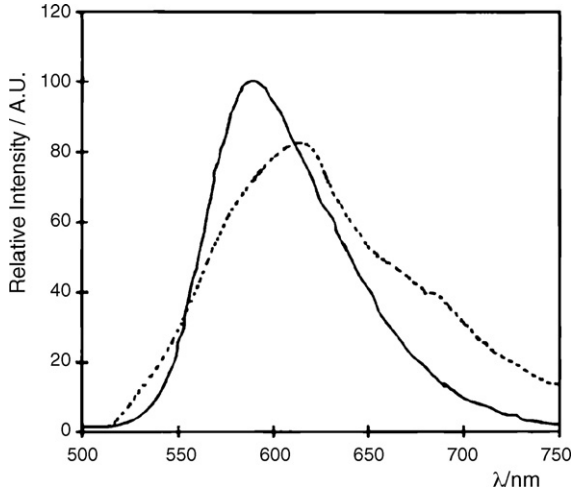

Fig. 20. Room-temperature emission spectra for $[Ru(bpy)_2Qbpy]^{2+}$ dissolved in 4:1 ethanol:methanol (s) and as a spontaneously adsorbed monolayer (- - -). In the case of the monolayer, the contacting solvent is 4:1 ethanol:methanol. The *y*-axes are normalized relative to each peak's maximum emission intensity [52].

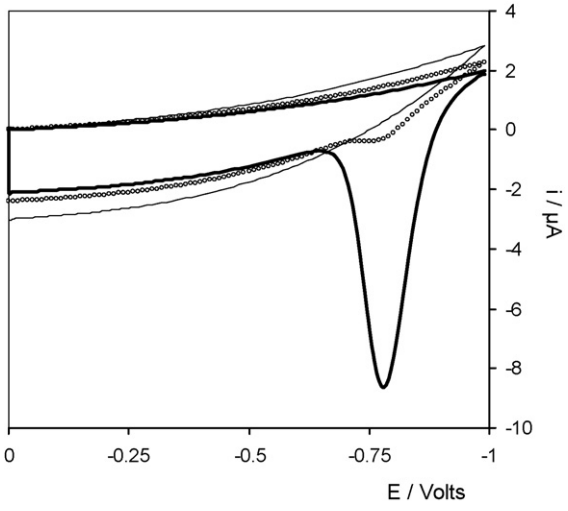

Fig. 21. Cyclic voltammetry of a 5 μm radius platinum microelectrode modified with an $[Ru(dpp)_2Qbpy]^{2+}$ monolayer following laser excitation at 355 nm (thick solid line). The open circles illustrate the second scan following laser excitation. The dashed line illustrates the voltammetric response obtained for a bare electrode under identical conditions. The scan rate is 3×10^5 V s^{-1}, the surface coverage is 1.1×10^{-10} mol cm^{-2} and the supporting electrolyte is 0.1 M $TBABF_4$ in acetonitrile [55].

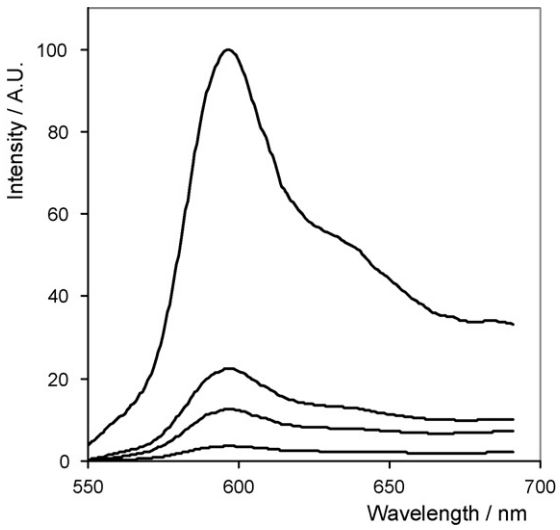

Fig. 22. Effect of partially oxidizing an $[Ru(dpp)_2Qbpy]^{2+}$ monolayer deposited on a 3 mm radius platinum microelectrode in contact with an aqueous 0.1 M $LiClO_4$ solution on the emission spectrum. From top to bottom the percentage of Ru^{3+} centers is 0, 3.7, 6.5 and 11 [55].

For example, the emission intensity decreases by more than 90% when only approximately 10% of the luminophores within the film are oxidized. This result indicates that the Ru^{3+} species acts as an efficient electron acceptor and quenches the emission, i.e., $Ru^{2+*} + Ru^{3+} \rightarrow Ru^{3+} + Ru^{2+}$. Given that the luminophores are bound within a supramolecular assembly, it is likely that quenching by Ru^{3+} occurs predominantly through a static mechanism.

Fig. 23 illustrates the Stern–Volmer plot which is highly linear and has a slope, K_{SV}, of $105 \pm 7\ M^{-1}$. The quantum yield of emission is proportional to the emission intensity, so that the Stern–Volmer equation can be expressed as

$$\frac{I_0}{I} = 1 + k_q \tau_0 [Ru^{3+}] \quad (2)$$

The excited-state lifetime for the complex in solution is $12.4 \pm 1.9\ \mu s$ and 392 ± 21 ns at 77 and 298 K, respectively. Taken in conjunction with the Stern–Volmer constant, the electron-transfer rate constant is between 8×10^6 and $3 \times 10^8\ M^{-1}\ s^{-1}$. This rate constant compares favorably with those reported elsewhere for ruthenium polypyridyl complexes in solution, solids and thin films [56–60]. However, when describing lateral quenching it is more appropriate to consider the process as occurring in two-dimensional space. The 3D k_q values above can be converted to 2D values using the following expression [61]:

$$^{3D}k_q = {}^{2D}k_q 2R \quad (3)$$

where R is the radius of an excluded volume encompassing both reactants. Assuming $R = 2r$ where r is the radius of the ruthenium complex (6.9 Å), leads to $^{2D}k_q$ values between 3×10^{16} and $1 \times 10^{18}\ cm^2\ mol^{-1}\ s^{-1}$. These data indicate that for close packed monolayers, Ru^{3+} is a highly efficient excited-state electron acceptor with rates that rival rates found in solution.

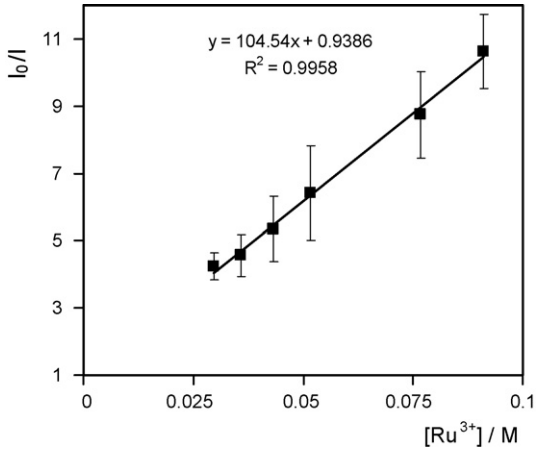

Fig. 23. Dependence of I_0/I on the Ru^{3+} quencher concentration for $[Ru(dpp)_2Qbpy]^{2+}$ monolayers in contact with aqueous 0.1 M $LiClO_4$. The intensity ratio is corrected for the change in Ru^{2+} concentration since the Ru^{3+} is created electrochemically [55].

Gulino et al. recently reported a strategy to reduce lateral quenching as a result of self-aggregation of metalloporphyrins in self-assembled monolayers, Fig. 24(a) [62]. The use of peripheral substituents to increase molecular bulk and steric hindrance around the luminophore prevents self-aggregation effects. The resulting SAMs were stable and exhibited photophysical properties which resembled those in solution.

Other examples of luminescent monolayers assembled from surface active metal complexes include mixed monolayers of ferrocene-thiol and Zn tetraarylporphyrin-thiol. Fluorescence was observed under open circuit condition and the quantity of photostored charge determined [63]. The influence of nanoscale metal features, i.e., surfaces or nanoparticles, on the photophysics of an assembled species has been considerably less studied than 2D arrays on extended planar surfaces. This situation arises because it has been widely held that such substrates efficiently quench the excited state of an assembled chromophore. In particular, if the energy of the luminescent transition lies below the surface plasmon (SP) frequency of the metal, the decay probability for the excited-state molecule is enhanced through strong coupling of the electronic transition dipole of the excited molecule with the surface plasmon field. This mechanism is reminiscent of Förster energy transfer in molecular systems. However, studies at both planar and nanoparticle metal surfaces have demonstrated this is not always the case. Nanoparticles are particularly important in photonic applications ranging from imaging to sensing and the ability to tune their optical properties with size and shape and through chemical modification is particularly attractive. A number of studies of coordination chromophores on nanoparticles have been described, to date, these have principally focused on ruthenium and osmium polypyridyl complexes.

Huang and Murray reported electrostatic binding of $[Ru(bpy)_3]^{2+}$ to gold nanoparticles functionalized with *N*-(2-mercaptopropionyl)glycine. This binding was accompanied by extensive static quenching of the $[Ru(bpy)_3]^{2+}$ luminescence, ascribed to energy transfer which could be reversed by addition of electrolyte, most notably Ca^{2+} ions [64]. Subsequently, Franzen et al. exploited time correlated single photon counting to quantify the direct binding of $[Ru(bpy)_3]^{2+}$ and $[Os(bpy)_3]^{2+}$ to gold and silver nanoparticles stabilized with either citrate or mercaptooctanoate [65]. Once bound, the luminescence of $[Ru(bpy)_3]^{2+}$ and $[Os(bpy)_3]^{2+}$ was significantly quenched and showed short, sub-nanosecond biexponential luminescence decay, which contrasted sharply with lifetime of metal complex in solution. The extent to which the stabilizing nanoparticle layer is displaced by the metal complex depends strongly on the identity of the stabilizing layer. Unsurprisingly, citrate was significantly more easy to displace than mercaptooctanoate. The quenching of $[Ru(bpy)_3]^{2+}$ and $[Os(bpy)_3]^{2+}$ by the nanoparticles was, on the basis of kinetic and thermodynamic arguments, ascribed to an electron-transfer process.

Fig. 25 illustrates the covalent attachment of ruthenium polypyridyl complexes functionalized with thiol tails onto gold nanoparticles described by Thomas et al. Here, the complexes were

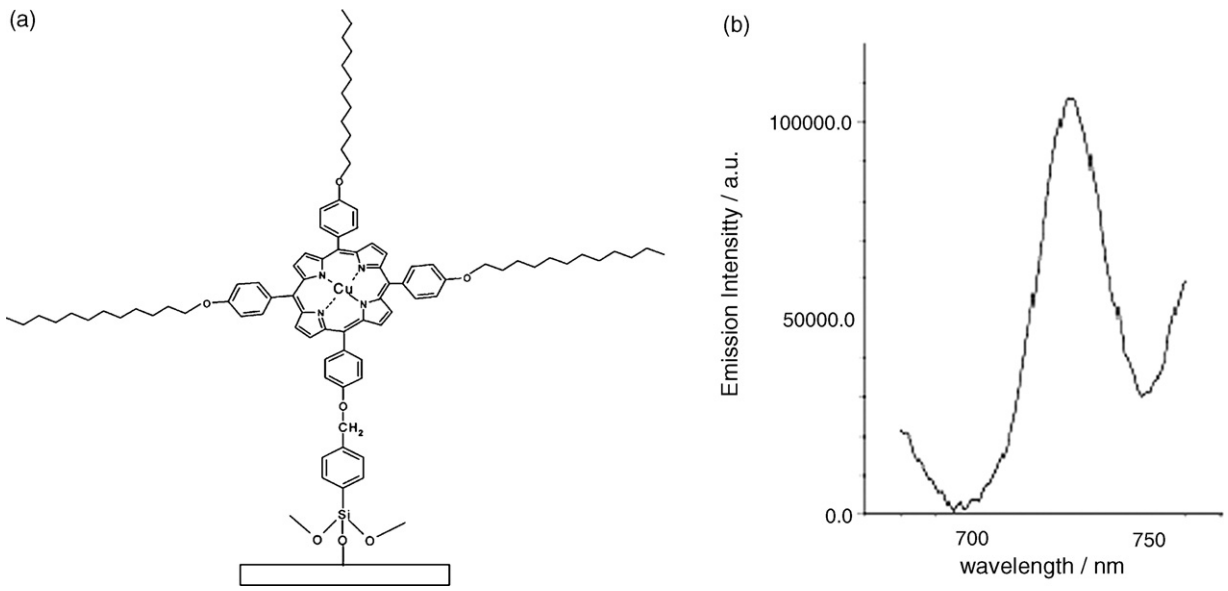

Fig. 24. (a) Structure of silylated 5,10,15-tri-(*p*-dodecanoxyphenyl)-20-(*p*-hydroxyphenyl) copper porphyrin assembled onto silica. (b) Luminescence spectrum of this SAM excited at 425 nm under an N_2 atmosphere [62].

assembled by exchange with thiol terminated triethylene glycol with which the nanoparticles were stabilized [66]. The ruthenium complexes retained their luminescence at the nanoparticle surfaces, and the photophysical properties could be tuned by altering the density of ruthenium centers at the nanoparticle surface. Lateral electron transfer between ruthenium centers was deemed responsible for a short component in the biexponential luminescent decay of the nanoparticle hybrids. The percentage contribution of this component decreases with decreasing ruthenium loading at the surface and transient absorption spectra was used to characterize the electron-transfer products, the processes are summarized in Fig. 25.

As shown in Fig. 26, the authors subsequently examined the photophysical behavior of these ruthenium-based luminophores on gold nanorods modified with *n*-dodecanethiol [67]. Assembly of the ruthenium centers caused significant modification to the absorbance spectrum of the nanorod plasmon suggests morphological changes induced by the ruthenium center. TEM also suggests some aggregation of the structures. Interestingly, unlike the spherical nanoparticles, the dominant quenching mechanism

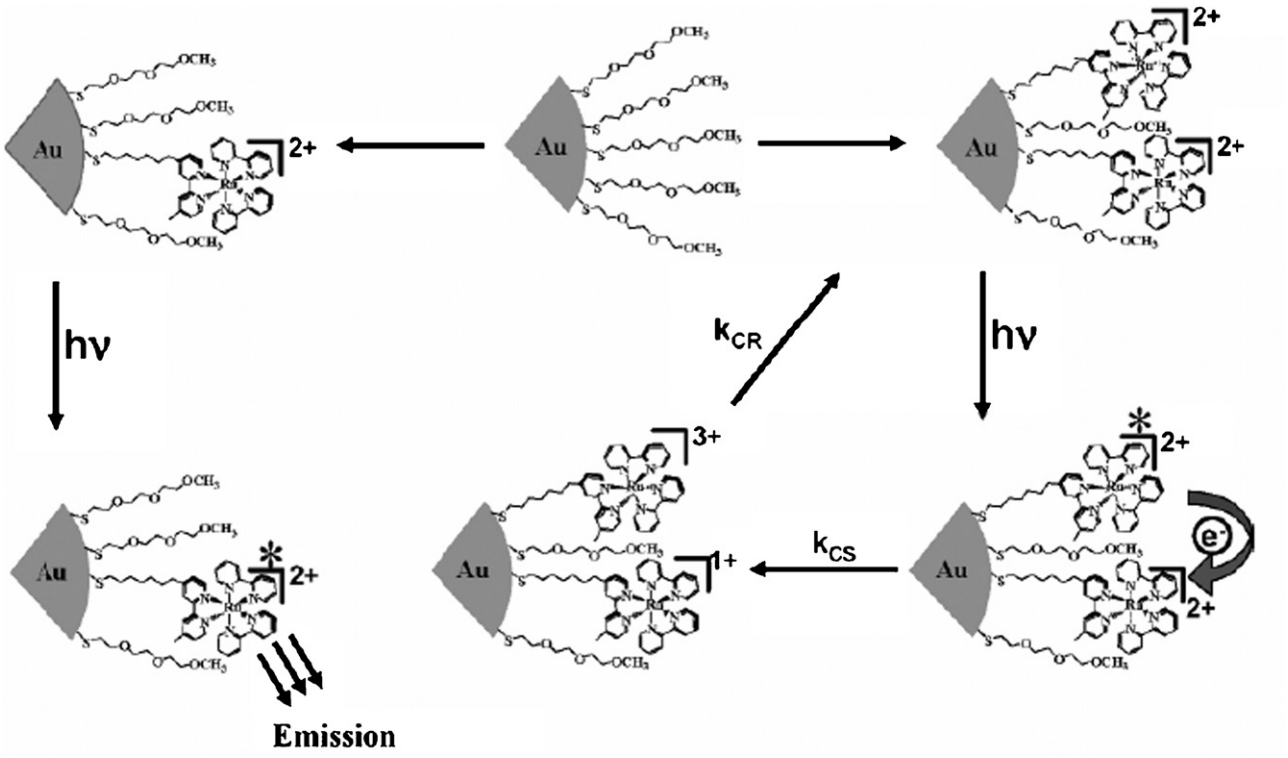

Fig. 25. Schematic of photoinduced concentration quenching Au(S–C7–Ru) and Au(S–C7–Ru)L, where k_{cs} and k_{cr} are rate constants for charge separation and recombination [66].

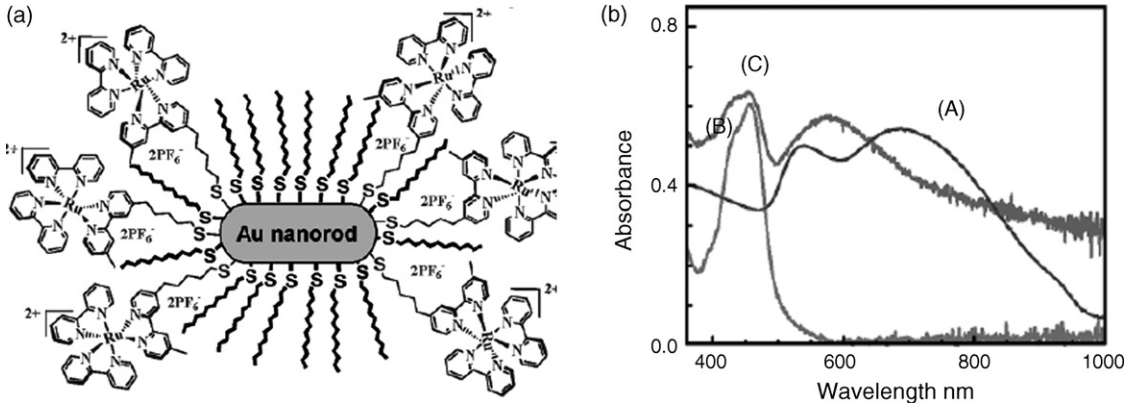

Fig. 26. (a) Schematic of gold nanorods with co-adsorbed $Ru(bpy)_3^{2+}$–C_5SH and *n*-dodecanethiol. (b) Absorption spectra of (A) Au-nanorods in *n*-dodecanethiol, (B) $Ru(bpy)_3^{2+}$–C_5–SH in dichloromethane (single peak centred at 450 nm), and (C) Au rod–Ru(II)thiol dye in dichloromethane after purification [67].

is *energy* transfer to the nanorods which occurred with a rate constant $>10^{10}\ s^{-1}$. Transient absorption spectroscopy confirmed that intermolecular electron transfer was not observed and this was attributed to the low loadings of the ruthenium centers on the nanorods.

Metal-based luminescent monolayers on non-conducting media, such as quartz, silica and mica, have also been reported. In the absence of a conducting surface however an important route to addressability is lost. Nonetheless, such assemblies serve to highlight the effect of close-packing and lateral interaction on the photophysical properties of a luminophore without the complication of direct surface interactions. For example, Fig. 27 shows luminescent monolayers reported by Di Bella et al. based on Schiff-base complexes assembled through a two-step assembly process on hydroxylated quartz substrates [68]. The materials retained their luminescence within the monolayer and did not appear to be prone to concentration quenching which might be expected in a close packed luminescent monolayer.

The electron-transfer rate across luminescent monolayers may also be modulated by chemical species, e.g., pH. For example, the imidazole moiety can be protonated/deprotonated in the $[Ru(bpy)_2PIC](PF_6)_2$ monolayers illustrated in Fig. 28 where bpy is 2,2′-bipyridyl and PIC is 2-(4-carboxyphenyl)imidazo[4,5-f][1,10]phenanthroline. These materials form luminescent self-assembled monolayers on fluorine doped tin oxide, through the carboxy terminus. Ionization of the imidazo bridge modifies the interfacial heterogeneous electron-transfer rate and the luminescence intensity and λ_{max} of the film [69]. The heterogeneous electron-transfer rate constant, measured at an overpotential of +50 mV, decreased from $7.0 \pm 1.1 \times 10^5$ to $0.7 \pm 0.1 \times 10^5\ s^{-1}$ as the pH of the supporting electrolyte was increased from 1.7 to 9.3. These observations were attributed to a superexchange electron-transfer process where the (carboxyphenyl)imidazo bridge plays an important mediating role in the redox switching process. The persistence of luminescence at this monolayer, despite its close proximity to the conducting surface was attributed to the fact that the excited state lies on the bipyridyl moieties which are not strongly coupled to the FTO states.

An important application of luminescent films is in sensing. Ruthenium polypyridyl complexes are well established in O_2 sensing and materials ranging from sol–gel and polymer matrices to zeolite have been exploited to immobilize the complexes in sensing devices. Interfacial films of ruthenium(II) 4,7-diphenyl-1,10-phenanthroline complexes were recently reported by Chu and Yam [70] who compared the efficiency of Langmuir–Blodgett films and self-assembled monolayers of the ruthenium complexes on glass for O_2 sensing. In each instance, oxygen quenching of the film luminescence was efficient, with relatively good dynamic response and reversibility. The authors ascribed this to the efficient diffusion of oxygen to the luminophores in this planar arrangement, and the exposure of the luminophores to the environment.

As described above, polyoxometalates are a versatile class of inorganic metal oxide clusters, which have been widely applied in electrostatic layer-by-layer assembly. The lanthanopolyoxometalates are a class of luminescent polyoxometalates. The luminescence arises from lanthanide addenda. Lanthanopolyoxometalates have been applied to the formation of luminescent multilayer assemblies. For example, Wang et al. reported on

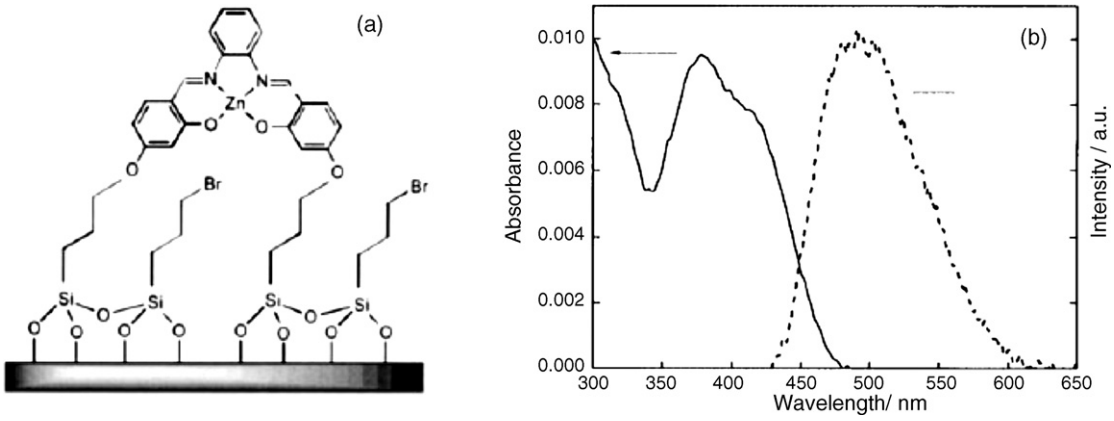

Fig. 27. (a) Structure of self-assembled monolayers of the Zn(II) Schiff-base complex on hydroxylated quartz substrates and (b) resulting absorbance and emission spectra [68].

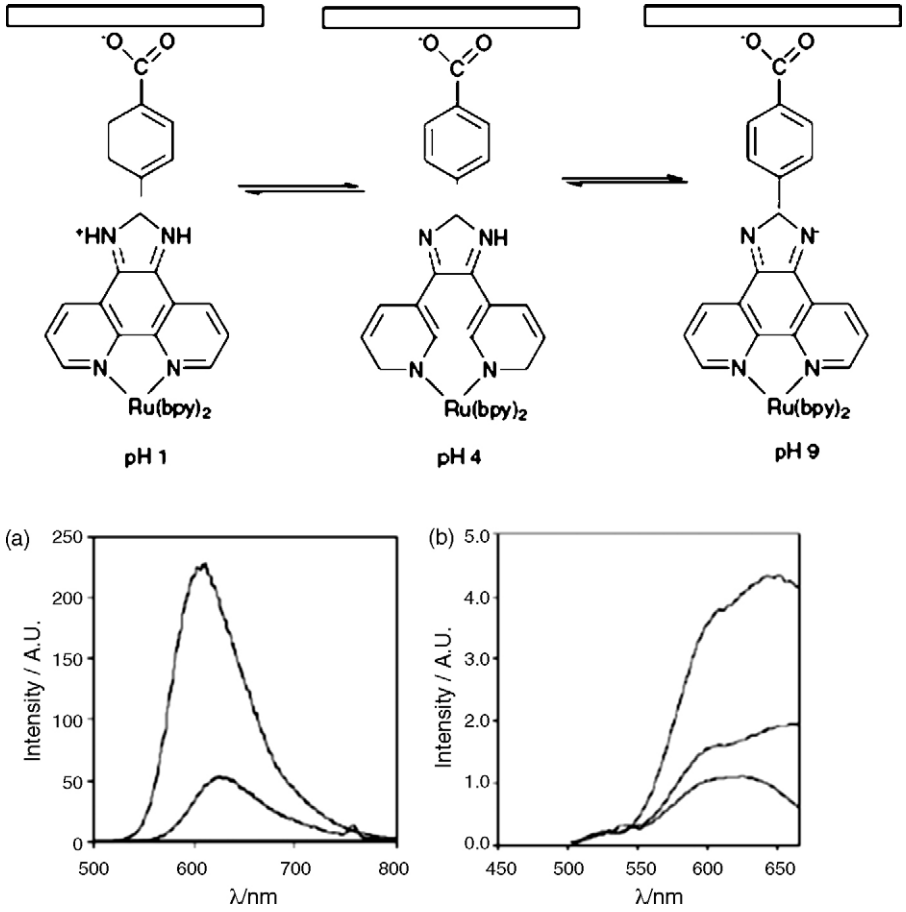

Fig. 28. (Top) Scheme of pH dependence of monolayer of $[Ru(bpy)_2PIC]^{2+}$ at pH1, 4 and 9. (Bottom) (a) Emission spectra of $[Ru(bpy)_2PIC]^{2+}$ dissolved in aqueous solution at pH 4 (upper curve) and pH 1 (lower curve). (b) Emission spectra for an FTO electrode modified with a monolayer of $[Ru(bpy)_2PIC]^{2+}$. From top to bottom, the pH of the contacting solution is 4.0, 3.1 and 0.9 [69].

layer-by-layer assembly of $K_{12}[EuP_5W_{30}O_{110}]$ (EuP_5W_{30}) and poly(allylamine hydrochloride) (PAH) and on a precursor film of {PEI/PSS/PAH} (where PEI is poly(ethyleneimine) and PSS is poly(styrenesulfonate)) on quartz [71]. AFM was used to estimate a film thickness of 6.5 nm, corresponding to an average thickness of approximately 1.1 nm for a EuW_{30}/PAH layer pair. The films were photoluminescent at room temperature and showed a characteristic Eu^{3+} emission pattern shown in Fig. 29, reminiscent of the lanthanopolyoxotungstate in solution.

As illustrated in Fig. 30, Ma et al. subsequently reported on the electrocatalytic and photoluminescent properties of layer-by-layer assembled films of *tris*(1,10-phenanthroline)ruthenium and 12-molybdophosphoric acid, $[PMo_{12}O_{40}]^{3-}$ on PEI modified indium tin oxide glass [72]. The films exhibited electrocatalytic reduction of ClO_3^-, BrO_3^-,IO_3^-, and oxidation towards $C_2O_2^{4-}$. In addition, they exhibited a photoluminescence attributed to the $3d(\pi)^*$ transition of $[Ru(phen)_3]^{2+}$. Some interesting modifications to the luminescent behavior of the film were observed in comparison to solid $[Ru(phen)_3]^{2+}$, both the MLCT excitation and bands were blue shifted by approximately 11 nm. The authors concluded this was indicative of strong interactions between ruthenium complex and metal ion.

1.8. Electrogenerated chemiluminescence (ECL)

ECL [73] has been obtained from gold and ITO electrodes modified with a SAM of *tris*(2,2′-bipyridine)ruthenium(II) type centers linked via thiols [74,75], carboxy [76], and pyridine functionalities.

The wavelengths of maximum emission for optically and electrochemically driven processes are often different [75]. For example, Fig. 31 shows that excitation of a dry $[Ru(bpy)_2(bpySH)](PF_6)_2$ monolayer leads to a broad emission with maxima at 560 and 630 nm. This figure also shows the emission spectrum of the complex in a butyronitrile/acetonitrile 4:1 glass at 77 K. While the

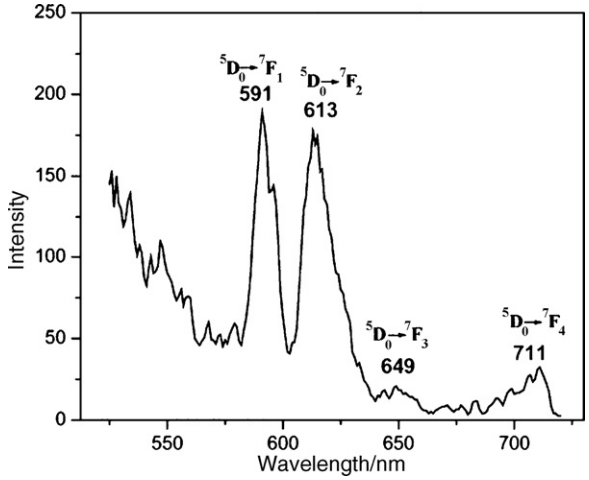

Fig. 29. Photoluminescence spectra (at 300 K) of EuW30/PAH multilayer film on quartz. The positions of 5D0 A7FJ ($J \sim 0$–4) emission bands are indicated in wavelength units (nm) [71].

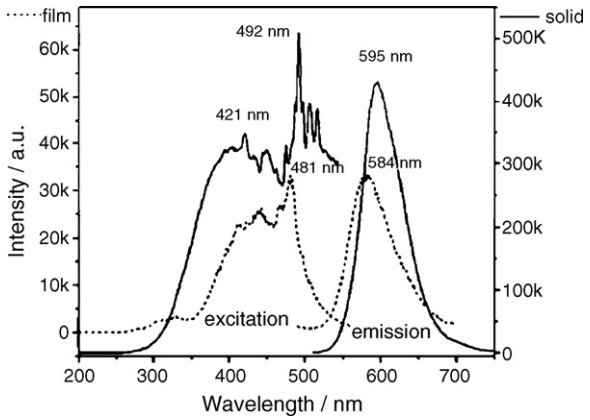

Fig. 30. Emission and excitation spectra of $Ru(phen)_3$ solid (solid lines) and {PEI/[PMo_{12}/$Ru(phen)_3$]$_{49}$}film (dotted lines) on quartz [72].

emission maximum of the main component is shifted to lower energy by approximately 30 nm, the overall emission envelope for the complex in a solid glass and dry monolayers are broadly similar. The emission profile is characteristic of Ru(II) *tris*-bipyridyl complexes, attributed to the closely lying levels of the excited state [77,78] ECL from the monolayer modified electrode was generated via the co-reactant pathway using tripropylamine dissolved in acetonitrile containing 0.1 M $TBABF_4$. Fig. 31 illustrates ECL spectra for a monolayer in which the surface coverage is 5×10^{-11} mol cm^{-2} after 48 h soaking in acetonitrile containing 0.1 M $TBAPF_6$. The spectrum was recorded in the absence of any dissolved complex. While there is significant noise in the data due to the small quantity of emissive material, a measurable emission centered at approximately 605 nm is observed.

Significantly, the emission profile differs from that observed for the dry monolayers and solid and is very similar to that observed for the complex dissolved in solution. This observation suggests that the monolayers become highly solvated when in contact with acetonitrile. The wavelength of maximum emission is similar to that observed for the complex dissolved in solution and is consistent with that found for the parent, $[Ru(bpy)_3]^{2+}$. Both the light-induced and electrochemiluminescence data indicate that monolayers of $[Ru(bpy)_2(bpySH)](PF_6)_2$ emit suggesting that the excited state is not strongly electronically coupled to the electrode surface.

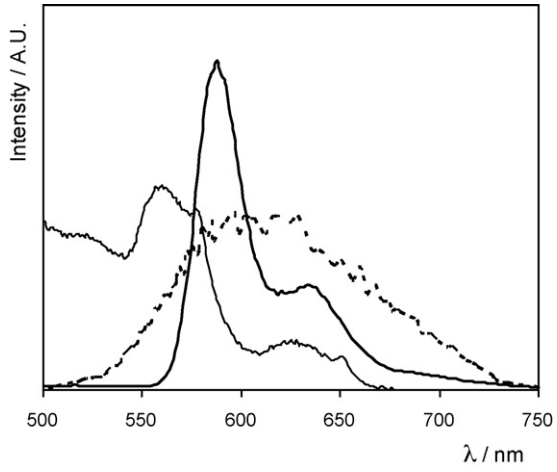

Fig. 31. Emission spectra of a dry RuBpySH monolayer on a 3 mm Pt electrode (—), λ_{exc} = 290 nm. Emission spectra of RuBpySH at 77 K in butyronitrile/acetonitrile 4:1; (▬) solution. ECL spectra (- - -) from an RuBpySH monolayer ($\Gamma = 5 \times 10^{-11}$ mol cm^{-2}) recorded following a potential step to 1.20 V. The solution contains 0.1 M $TBABF_4$ in acetonitrile and 0.1 M tripropylamine [75].

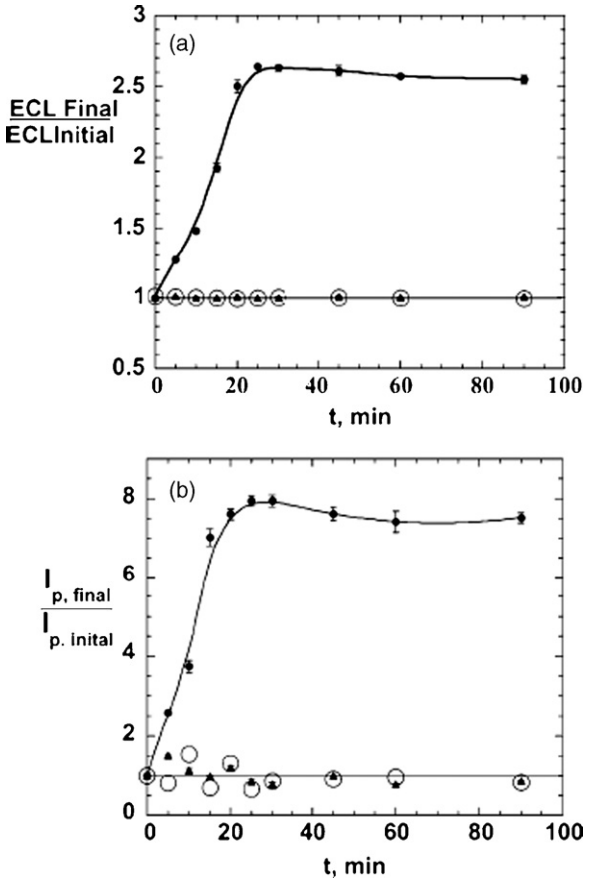

Fig. 32. Influence of incubation time with styrene oxide (●), toluene (▲), and buffer alone (○) on (a) average ECL signals and (b) average SWV catalytic peak currents (final response/initial response) for $(Ru/ds\text{-}CT\ DNA)_2$ films. Error bars represent standard deviations for three trials, with 1 electrode/trial [79].

Thin films of metallopolymers also generate quite intense ECL [79]. For example, direct electrochemiluminescence involving DNA has been demonstrated in 10 nm films of cationic polymer $[Ru(bpy)_2(PVP)_{10}]^{2+}$ assembled layer-by-layer with DNA [80]. Significant ECL is only observed in the presence of guanine bases suggesting that guanine radicals initially formed by catalytic oxidation of guanines by Ru(III) react with the metallopolymer to produce electronically exited $Ru(II)^*$ sites in the film. Both the current and light responses are sensitive to oligonucleotide hybridization and chemical DNA damage. For example, as shown in Fig. 32, incubation of DNA with the known DNA damage agent, styrene oxide, causes the ECL intensity to increase linearly over approximately 20 min. The estimated detection limit was 1 damaged DNA base in 1000.

Oxidative DNA damage leading to the formation of oxo-guanine, e.g., using Fenton reagent, can be detected by ECL generated at thin films of $[Os(bpy)_2(PVP)_{10}]^{2+}$ metallopolymer. Films combining DNA, $[Ru(bpy)_2(PVP)_{10}]^{2+}$, and $[Os(bpy)_2(PVP)_{10}]^{2+}$ had Os(II) sites that produced ECL specific for oxidized DNA, and Ru(II) sites gave ECL from reaction with oxo-adenines, chemically damaged DNA, and possibly from cleaved DNA strands [81]. Fig. 33 illustrates an interesting oscillation in the ECL and current intensity when $(OsRu\text{-}PVP/ds\text{-}DNA)_2$ films were incubated with Fenton reagent for various times. The initial increase may be attributed to the formation of oxidized adenine derivatives or possible strand breaks, either of which can result from the action of the Fenton reagents on DNA.

Other significant examples of monolayer promoted ECL exist. For example, Sato et al. investigated the electro-oxidative chemiluminescence from a luminol/hydrogen peroxide system catalyzed by a ferrocenethiol SAM-modified gold electrode. When luminol

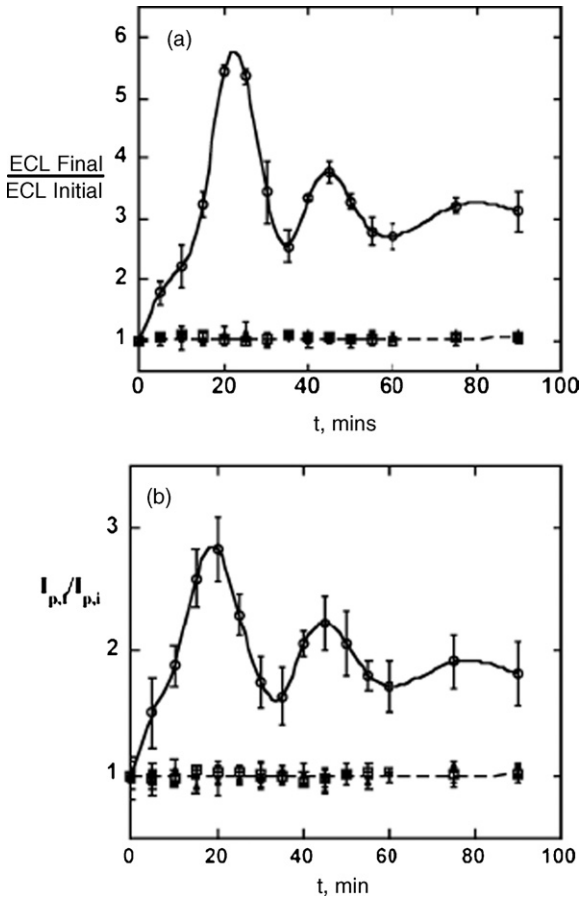

Fig. 33. Influence of incubation of $(OsRu\text{-}PVP/ds\text{-}ST\ DNA)_2$ films with Fenton reagent (○), with $FeSO_4$ alone (▲), H_2O_2 alone (□), and only pH 5.5 buffer (+) on (a) average ECL signals and (b) average SWV catalytic peak currents for the OsII/OsIII redox couple. Error bars represent standard deviations for three trials; one electrode was used per trial [80].

and hydrogen peroxide were contained in the electrolyte solution, in addition to an oxidation peak due to the redox of ferrocene, catalytic oxidation current of luminol was observed and light emission was simultaneously observed from the solution phase luminol. The system could be successfully used to detect glucose in the presence of glucose oxidase [82].

Stable self-assembled monolayers of $[Ru(bpy)_2dcb]Cl_2$ where dcb is 4,4′-dicarboxy-2,2′-bipyridine form readily on optically transparent electrode FTO to form luminescent films [83]. These materials produce significant ECL in response to oxalate and several amino acids in Fig. 34(b). For example, the linear range for ECL detection of proline was $0.2 \leq [Proline] \leq 1$ nM while for hydroxyproline the dynamic range was from 1 to 10 nM. As shown in Fig. 34(a), the ECL is shifted to the red (≈30 nm) by comparison with the luminescence from the film.

1.9. Photopatterning using SAMs

The trend towards nanoscale, integrated optoelectronic devices continues to drive the required resolution of patterning towards smaller and smaller length scales. Since Whitesides' seminal work on microcontact printing using SAMs of alkylsiloxanes, [84,85] there has been significant interest in photopatterning using alkane thiol-based SAMs [86–89]. While the majority of these approaches are not currently based on immobilized transition metal complexes, a couple of examples are included here because of they provide a method for patterning a surface that can be subsequently backfilled with an optically active SAM, for example to create a photonic crystal. Moreover, there appear to be particular advantages in using surface active metal complexes for patterning, e.g., individual components can be selectively addressed within a multi-component system on the basis of the absorbance spectra.

Fig. 35 illustrates the high-resolution patterning approach developed by Crooks and co-workers [90]. First, a transmission electron microscope (TEM) minigrid was placed as a photomask on top of a closed-packed $HOOC–(CH_2)_{10}–C{\equiv}C–C{\equiv}C–(CH_2)_{10}–SH$ SAM on a Au/Cr/Si surface. Exposure of the entire modified surface to UV irradiation induces polymerization in the unmasked regions of the SAM. Significantly, the photopolymerized film is more stable film and, unlike the parent monolayer, resists electrochemical desorption. Therefore, the non-polymerized portion of the monolayer resist can be selectively desorbed using an electrochemical reductive stripping method. Removing the resist creates a negative image of the mask, which can be elaborated by etching the grid image into the Au surface with an O_2-saturated 1 M KOH + 10 mM KCN aqueous solution.

At the micron length scale the reproduction of the mask features is excellent. However, close inspection reveals that the lateral dimensions of the hexagonal raised regions are *less* than those of the original mask. This may arise from diffraction off the mask

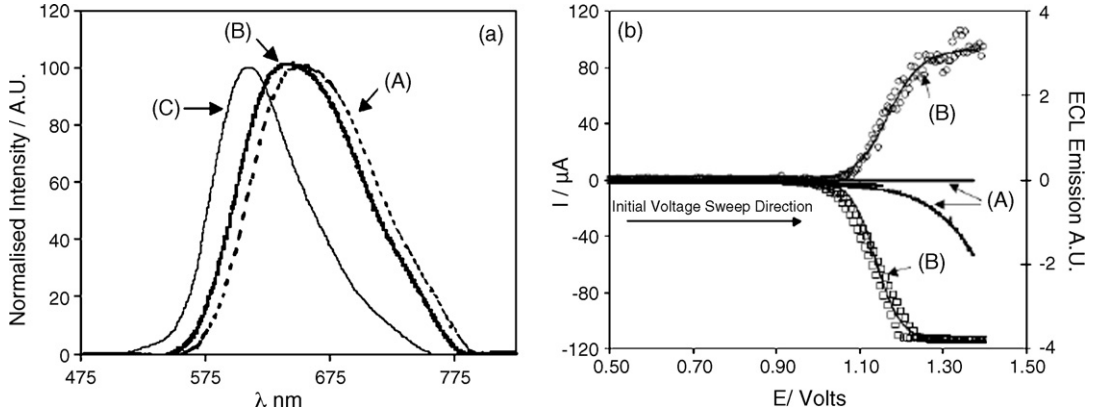

Fig. 34. (a) ECL spectrum (B) of monolayer on FTO electrode in contact with a solution containing 0.1 M H_2SO_4 and approximately 10 mM oxalate. The ECL spectrum (A) of monolayer on FTO electrode in contact with a solution containing 0.5 M H_3BO_3 and approximately 10 mM proline (pH 9.8). The photoluminescence spectrum (C) of the monolayer on FTO in contact with 0.1 M H_2SO_4. Excitation was by means of a 10 ns laser pulse (355 nm). (b) Potential dependence of current and emission intensity of an unmodified (A) and modified (B) electrode in 0.4 M Na_2SO_4 solution containing 10 mM $Na_2C_2O_4$ (pH 4.7). Scan rate of 100 mV s^{-1}. Scan is started at a potential of 0.5 V and the arrow indicates the direction of the initial voltage sweep [83].

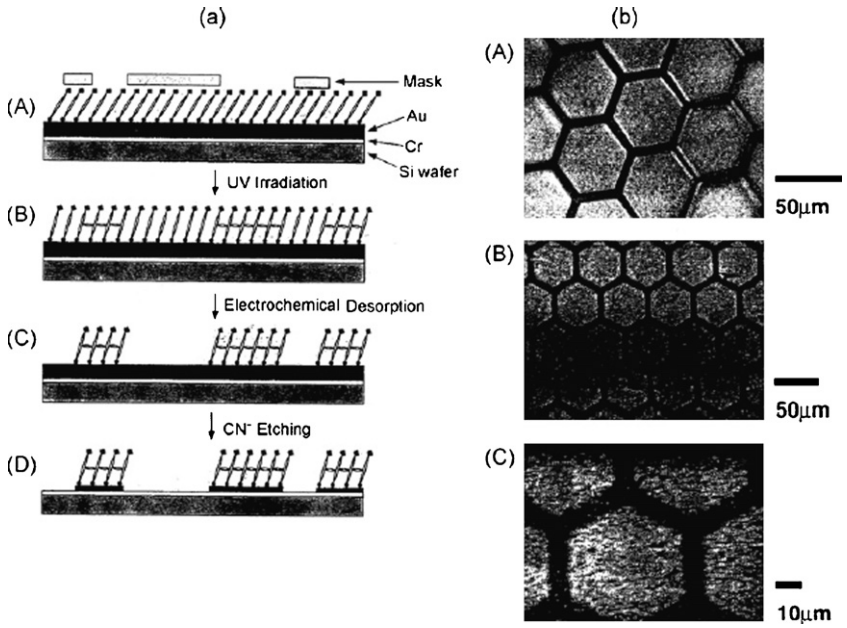

Fig. 35. (a) Schematic of patterning approach. (b) (A) is an optical micrograph of a 400-mesh (holes per linear inch) Cu TEM minigrid, which was used to pattern the Au surface. (B) and (C) are scanning electron micrographs (SEMs) of a patterned Au surface [90].

edges, that is, from the modulation transfer function, which will tend to reduce the photon flux in areas near the vicinity of the mask edges. Other approaches include scanning near-field photolithography technique in which a near-field scanning optical microscope (NSOM) coupled to a UV laser is used to selectively oxidize alkylthiols in SAMs [91]. The weakly bound alkylthiolate oxidation products may either be replaced by a ligand exchange reaction to yield patterned structures as small as 20 nm. There appear to be no barriers to using surface active transition metal complexes in this step to create patterned photonic crystals. Alternatively, etching of the pattern yields three-dimensional structures within the underlying substrate.

2. Conclusions and future directions

The use of molecular self-assembly for creating mono- and multilayer structures at interfaces has come a long way since the initial alkane thiol assemblies were reported. The extent of structural control, functionality and architectural diversity of interfacial structures reported across today's literature is truly impressive. Here, examples of SAM formation, layer-by-layer assembly and coordination driven multilayer formation methods have been discussed in the context of coordination compounds.

Transition metal complexes often exhibit well-behaved redox and photochemical properties making them attractive building blocks for arrays. In turn, these properties allow the properties of the assemblies to be probed (READ function) or purposefully modified (WRITE function). In addition, coordination chemistry is frequently facile, and can be used to build organized 2D and 3D architectures under ambient conditions if suitable ligands can be built into a film. Coordination compounds also have other interesting photochemically driven properties ranging from ligand substitution and isomerization to photocatalysis which may find use in interfacial architectures. Possible areas for application of such functions include photopatterning for nanofabrication for lithography or sensing arrays to redox or photoredox mediation of interfacial electron transfer in biological assemblies. However, the field remains dominated by organic architectures. Over the coming years it is likely that photoactive coordination compounds will play an greater role in interfacial photonic architectures as the synthetic versatility and robustly predictable redox/photochemical properties of such materials is increasingly appreciated.

2.1. New and emerging applications

The first proof-of-concept devices using photonic interfacial supramolecular assemblies incorporating transition metals have already been demonstrated and are poised to reap their first commercial benefits within the next 10 years. These applications include high-resolution spectral filters for fiber optic telecommunications, all-optical switches, light-emitting diodes (LEDs), photonic-crystal thin films to serve as anti-counterfeit protection on credit cards, biosensors and light generators and detectors. A longer range goal is to use these components to construct an all-optical computer.

2.1.1. Molecular electronics

The ability to control the flow of electrons in semiconductors led to the current explosion in information technology. Photonic crystals promise similar control over photons. These photonic crystals typically consist of holes within a dielectric layer arranged in a lattice-like structure and repeated identically and at regular intervals. When built with sufficient precision, these crystals exhibit a photonic bandgap, i.e., a range of frequencies within which a specific wavelength of light is blocked. Interfacial photonic arrays offer an alternative approach to creating photonic bandgaps but with the added advantage that the properties of the crystal can be controlled by tuning the ground and excited-state photonic properties of the transition metal complex and the structure can be self-assembled rather than rely on complex and often expensive nanolithographic techniques. Self-assembly offers some advantages over current nanoscale fabrication techniques. For example, the high intensity of the EUV beam sources leads to degradation of the components which decreases their lifetime and the poor reflectivity of others limits the potential of the processes. Another advantage of self-assembly is that it can be used to create three-dimensional structures by using then templating capabilities of metal ions, for example, through a vacant coordination site or by coupling through the functional group of a bound ligand. This molecular level and flexible control contrasts with con-

ventional nanoscale lithographic techniques. The excellent work on the self-assembly of a large variety of supramolecular systems that have potential photonic, magnetic, catalytic, and analytical properties has been well matched by the development of physical methods to characterize these systems on the nanometer scale. The potential usefulness and functionality of interfacial photonic arrays has been well documented through proof of principle experiments, such as those using scanning-probe tips to construct and evaluate the device. However, in general, the methods to incorporate these nanoscaled self-assembled materials or objects into devices on a production (economically feasible) scale have significantly lagged behind. It is now recognized that although it is a burgeoning area of materials research, these self-assembled systems will have to subsequently, or concomitantly, self-organize into hierarchical structures that may also form the interconnects to the macroscopic world. For many of these devices based on organic or hybrid inorganic–organic compounds, in analogy to biological systems, the primary, secondary, tertiary, and quaternary levels of structural organization will need to be controlled. The properties of the primary structure or building block, e.g., a metal complex capable of coupling to adjacent units through electrostatic or bonding interactions, can be exquisitely controlled. The pioneering work of Pedersen, Cram, and Lehn almost 30 years ago underpins approaches to controlling the way that these building blocks self-assemble to give a secondary structure on the scale of less than a few nanometers. The tertiary structure, i.e., how the self-assembled supermolecules self-organize into entities that are many tens to hundreds of nanometers in at least one direction, has progressed rapidly. Lastly, the quaternary structure involving the architecture of the self-organized systems in the actual device or material requires additional attention.

2.2. Expected applications and technologies within next 10 years

While only a small fraction of their ultimate performance has been realized, photonic technologies based on interfacial photonic arrays based on transition metal complexes, promise to contribute significantly to vital societal objectives. These include high-speed telecommunications, improving health care as well as helping people live longer, healthier lives through advanced diagnostic devices as well as producing and saving energy. Significantly, photonics has a tremendous leverage for creating products in a broad range of industrial sectors that multiply the value of initial photonic components and technologies many times over.

2.2.1. Information storage

A key technical challenges is to further increase both the information storage density and data transfer rates to enable new applications such as digital storage for mobile digital devices (e.g., still picture cameras, camcorders, multi-functional mobile phones, mp3 players, handheld computers, PDA, game consoles), super high-quality video (beyond HD-TV) distribution and economic long-term data archiving. Fourth generation technologies will target a capacity between 250 and 500 GB on a CD sized disc. In spite of the impressive progress that optical storage technologies have already made at the heart of our information society, storage systems and devices are still in an early stage of their development. There continues to be intense efforts to create multibit photonic systems capable of storing information at the single molecule level. Particular advantages ought to accrue from combining metallic nanostructures with interfacial photonic assemblies. These approaches ought to allow the real density to be increased by combating the diffraction limits of write and read optics. For example by using near-field optics and SuperRENS (Super Resolution Near-field Structures). Of course, extending to 3D optical storage systems will dramatically increase the storage density.

2.2.2. Flat panel displays

There is significant interest in developing novel displays and lighting systems. Interfacial photonic arrays can be used as long-life materials for light-emission and even perhaps transparent transistors for see-through lighting and displays. Key objectives include flexible substrates, appropriate encapsulation, packaging, interconnects, hybrid organic/inorganic electronic devices and improved light extraction from thin film devices.

2.2.3. Optical processing

Optical signal processing using the electronically excited-state properties of interfacial arrays of transition metal complexes, has the potential to realize high-speed and high-capacity processing at speeds which are 100–1000 times faster than that achievable with conventional electronic signal processing. For example, it ought to be possible to achieve ultrafast all optical switching by using a laser pulse that precedes an information packet to create the excited state of the metal complexes that is optically transparent at a given wavelength so as to allow the information pass into a fiber. Given the wide range of excited-state lifetimes available this approach might enable ultra high-speed networks, into the multi-terabit per second regime.

2.2.4. Biomedical

The classical approach to treating disease of first recognizing the symptoms, followed by a diagnosis and subsequent treatment, is changing. The emerging healthcare systems will be more proactive involving preventive screening, identification of a gene or upregulated protein followed by curative treatment or prophylaxis. Interfacial photonic interfacial supramolecular assemblies incorporating transition metals will play an important role in developing sensors to underpin this strategy. Photonics plays a key role in the biochemical and environmental sensing domain because of the many ways in which light can interact with target analytes. Specifically, in the case of interfacial photonic arrays of transition metal complexes binding groups ranging from antibodies, DNA and synthetic receptors can be introduced making the array selective for the target molecule. These bound molecules can then be detected through changes in the refractive index upon binding or fluorescence using either the target molecule's intrinsic fluorescence or an appropriate fluorescent tag. The exquisite sensitivity of optical detection strategies ranging from optically driven emission to electrochemiluminescence places them at the forefront of strategies to detect picomolar concentrations of biomarkers in nanolitre volumes of blood.

In closing, current fundamental limits must be overcome with basic research on light–matter interactions and on novel materials and structures, such as interfacial arrays of transition metal complexes, that have revolutionary photonic properties. This will open up the way to groundbreaking new optical components and the corresponding technologies for their fabrication. The goal of conquering the limitations of current optical elements will only be realized through a combination of many scientific competencies including chemistry, material science, quantum optics, thermodynamics and solid-state physics. The physical and technical limitations of optics components can only be resolved with interdisciplinary research efforts in the fields of interfacial self-assembly, micro-system engineering, nanotechnology, coupled to specialists in application domains as diverse as telecommunications and sensors.

Acknowledgement

The support of the Higher Education Authority of Ireland for funding under the Programme for Third Level Institutions is gratefully acknowledged.

References

[1] A.P. Alivisatos, P.F. Barbara, A.W. Castleman, J. Chang, D.A. Dixon, M.L. Klein, G.L. McLendon, J.S. Miller, M.A. Ratner, P.J. Rossky, Adv. Mater. 10 (1998) 1297.
[2] J.-M. Lehn, Pure Appl. Chem. 66 (1994) 1961.
[3] P.J. Stang, B. Olenyuk, Acc. Chem. Res. 30 (1997) 502.
[4] D. Philp, J.F. Stoddart, Angew. Chem. Int. Ed. Engl. 35 (1996) 1154.
[5] A. Aviram, M.A. Ratner (Eds.), Molecular Electronics Science and Technology, New York Academy of Science, New York, 1998.
[6] R. Daganni, Chem. Eng. News 76 (1998) 35.
[7] K. Ariga, J.P. Hill, M.V. Lee, A. Vinu, R. Charvet, S. Acharya, Sci. Technol. Adv. Mater. 9 (2008) 014109.
[8] H.O. Finklea, in: A.J. Bard, I. Rubinstein (Eds.), Electroanalytical Chemistry, Marcel Dekker, New York, 1996, p. 109.
[9] H.O. Finklea, in: R.A. Meyers (Ed.), Encyclopedia of Analytical Chemistry, Wiley & Sons, Chichester, 2000, p. 10090.
[10] D. Acevedo, H.D. Abruña, J. Phys. Chem. 95 (1991) 9590.
[11] R.J. Forster, P.J. Loughman, T.E. Keyes, J. Am. Chem. Soc. 122 (2000) 11948.
[12] R.J. Forster, L.R. Faulkner, J. Am. Chem. Soc. 116 (1994) 5444.
[13] R.J. Forster, L.R. Faulkner, J. Am. Chem. Soc. 116 (1994) 5453.
[14] R.J. Forster, Y. Pellegrin, D. Leane, J. Brennan, T.E. Keyes, J. Phys. Chem. C 111 (2007) 2063.
[15] E. Ruckenstein, Z.F. Li, Adv. Coll. Interf. Sci. 113 (2005) 43.
[16] G. Decher, J. Hong, J. Schmitt, Thin Solid Films 210 (1992) 831.
[17] G. Decher, Science 29 (1997) 1232.
[18] K. Ariga, J.P. Hill, Q. Ji, Phys. Chem. Chem. Phys. 9 (2007) 2319.
[19] A. Kuhn, F.C. Anson, Langmuir 12 (1996) 5481.
[20] G. Gao, L. Xu, W. Wang, W. An, Y. Qiu, Z. Wang, E. Wang, J. Phys. Chem. B 109 (2005) 8948.
[21] S. Liu, D. Volkmer, D.G. Kurth, Anal. Chem. 76 (2004) 4579.
[22] M. Wanunu, A. Vaskevich, S.R. Cohen, H. Cohen, R. Arad-Yellin, A. Shanzer, I. Rubinstein, J. Am. Chem. Soc. 127 (2005) 17877.
[23] H. Krass, G. Papastavrou, D. Kurth, Chem. Mater. 15 (2003) 196.
[24] J.A. Zasadzinski, R. Viswanathan, L. Madsen, J. Garnaes, D.K. Schwartz, Science 263 (1994) 1726.
[25] R.J. Forster, T.E. Keyes, J.G. Vos, Interfacial Supramolecular Assemblies, Wiley, Chichester, 2003, 193 (Chapter 5).
[26] A.M. Kuznetsov, J. Ulstrup, Electron Transfer in Chemistry and Biology, An Introduction to the Theory, Wiley, Chichester, 1999.
[27] G.J. Kavernos, Fundamentals of Photoinduced Electron Transfer, Wiley, Chichester, 1993.
[28] J. Deisenhofer, O. Epp, K. Miki, R. Huber, H. Michel, J. Mol. Biol. 180 (1984) 385.
[29] P. Seta, E. Bienvenue, A.L. Moore, P. Mathis, R.V. Bensasson, P. Liddell, P.J. Pessiki, A. Joy, T.A. Moore, Nature 316 (1985) 653.
[30] Y. Sakata, H. Tatemitsu, E. Bienvenue, P. Seta, Chem. Lett. (1988) 1625.
[31] M. Fujihira, Mol. Cryst. Liq. Cryst. 183 (1990) 59.
[32] K. Uosaki, T. Kondo, X.-Q. Zhang, M. Yanagida, J. Am. Chem. Soc. 119 (1997) 8367.
[33] H. Imahori, H. Yamada, Y. Nishimura, I. Yamazaki, Y. Sakata, J. Phys. Chem. B 104 (2000) 2099.
[34] A. Ishida, T. Majima, Nanotechnology 10 (1999) 208.
[35] A. Ikeda, T. Hatano, S. Shinkai, T. Akiyama, S. Yamada, J. Am. Chem. Soc. 123 (2001) 4855.
[36] F.B. Abdelrazzaq, R.C. Kwong, M.E. Thompson, J. Am. Chem. Soc. 124 (2002) 4796.
[37] S.B. Ungashe, W.L. Wilson, H.E. Katz, G.R. Scheller, T.M. Putvinski, J. Am. Chem. Soc. 114 (1992) 8717.
[38] S.W. Keller, H.N. Kim, T.E. Mallouk, J. Am. Chem. Soc. 116 (1994) 8817.
[39] P.G. Hoertz, T.E. Mallouk, Inorg. Chem. 44 (2005) 6828.
[40] E. Soto, J.C. MacDonald, C.G.F. Cooper, W.G. McGimpsey, J. Am. Chem. Soc. 125 (2003) 2838 (correction J. Am. Chem. Soc. 125 (2003) 4670).
[41] M. Brust, M. Walker, D. Bethell, D.J. Shiffrin, R. Whyman, J. Chem. Soc., Chem. Commun. (1994) 801.
[42] M. Brust, J. Fink, D. Bethell, D.J. Shiffrin, C. Kiely, J. Chem. Soc., Chem. Commun. (1995) 1655.
[43] M.J. Hostetler, A.C. Templeton, R.W. Murray, Langmuir 15 (1999) 3782.
[44] C. Drain, Proc. Natl. Acad. Sci. 99 (2002) 5178.
[45] B.C. Crandall, J. Lewis (Eds.), Nanotechnology, MIT Press, Cambridge, MA, 1992.
[46] D.G. Walter, D.J. Campbell, C.A. Mirkin, J. Phys. Chem. B 103 (1999) 402.
[47] C.G.F. Cooper, J.C. MacDonald, E. Soto, W.G. McGimpsey, J. Am. Chem. Soc. 126 (2004) 1032.
[48] E. Katz, B. Willner, I. Willner, Biosens. Bioelectron. 12 (1997) 703.
[49] B. Richie, E. Burstein, Phys. Rev. B 24 (1981) 4843.
[50] D.A. Weitz, S. Garoff, J.I. Gersten, A.J. Nitzan, J. Chem. Phys. 78 (1983) 5324.
[51] A. Wokuan, H.-P. Lutz, A.P. King, U.P. Wild, R.R. Ernst, J. Chem. Phys. 79 (1983) 509.
[52] R.J. Forster, T.E. Keyes, J. Phys. Chem. B 102 (1998) 10004.
[53] A.J. Bard, L.R. Faulkner, Electrochemical Methods: Fundamentals and Applications, Wiley, New York, 1980.
[54] R.J. Forster, Ultrafast Electrochemical Techniques, Encyclopedia of Analytical Chemistry, Wiley and Sons, New York, 1998.
[55] R.J. Forster, J.L. Brennan, T.E. Keyes, Langmuir 22 (2006) 10754.
[56] M. Majda, L.R. Faulkner, J. Electroanal. Chem. 137 (1982) 149.
[57] M. Majda, L.R. Faulkner, J. Electroanal. Chem. 169 (1984) 97.
[58] D.A. Buttry, F.C. Anson, J. Am. Chem. Soc. 104 (1982) 4824.
[59] M. Altamirano, A. Senz, H.E. Gsponer, J. Coll. Interf. Sci. 270 (2004) 364.
[60] M.D. Newsham, R.I. Cukier, D.G. Nocera, J. Phys. Chem. 95 (1991) 9660.
[61] D.H. Charych, E.M. Landau, M. Majda, J. Am. Chem. Soc. 113 (1991) 3340.
[62] A. Gulino, I. Fragalà, E. Scamporrino, D. Vitalini, J. Phys. Chem. C 111 (2007) 14125.
[63] K.M. Roth, J.S. Lindsey, D.F. Bocian, W.G. Kuhr, Langmuir 18 (2002) 4030.
[64] T. Huang, R.W. Murray, Langmuir 18 (2002) 7077.
[65] W. Glomm, S.J. Moses, M.K. Brennaman, J.M. Papanikolas, S. Franzen, J. Phys. Chem. B 109 (2005) 804.
[66] P. Pramod, P.K. Sudeep, K.G. Thomas, P.V. Kamat, J. Phys. Chem. B 110 (2006) 20737.
[67] M. Jebb, P.K. Sudeep, P. Pramod, K.G. Thomas, P.V. Kamat, J. Phys. Chem. B 111 (2007) 6839.
[68] S. Di Bella, N. Leonardi, G. Consiglio, S. Sortino, I. Fragalà, Eur. J. Inorg. Chem. (2004) 4561.
[69] R.J. Forster, Y. Pellegrin, T.E. Keyes, Electrochem. Commun. 9 (2007) 1899.
[70] B.W.-K. Chu, V.W.-W. Yam, Langmuir 22 (2006) 7437.
[71] L. Xu, H. Zhang, E. Wang, D.G. Kurth, Z. Li, J. Mater. Chem. 12 (2002) 654.
[72] H. Ma, T. Dong, G. Wang, W. Zhang, F. Wang, X. Wang, Electroanalysis 18 (2006) 2475.
[73] M.M. Richter, Chem. Rev. 104 (2004) 3003.
[74] Y. Sato, K. Uosaki, J. Electroanal. Chem. 384 (1995) 57.
[75] P. Bertoncello, Z. Pikramenou, P.R. Unwin, R.J. Forster, J. Phys. Chem. 110 (2006) 10063.
[76] L. Dennany, E. O'Reilly, R.J. Forster, Electrochem. Commun. 8 (2006) 1588.
[77] A. Juris, V. Balzani, F. Barigelletti, S. Campagna, P. Belser, A. von Zelewsky, Coord. Chem. Rev. 84 (1988) 85.
[78] J.V. Caspar, T.J. Meyer, J. Am. Chem. Soc. 105 (1983) 5583.
[79] L. Dennany, C.F. Hogan, T.E. Keyes, R.J. Forster, Anal. Chem. 78 (2006) 1412.
[80] L. Dennany, R.J. Forster, J.F. Rusling, J. Am. Chem. Soc. 125 (2003) 5213.
[81] L. Dennany, R.J. Forster, B. White, M.R. Smyth, J.F. Rusling, J. Am. Chem. Soc. 126 (2004) 8835.
[82] Y. Sato, T. Sawaguchi, F. Mizutani, Electrochem. Commun. 3 (2001) 131.
[83] L. Dennany, E.J. O'Reilly, T.E. Keyes, R.J. Forster, Electrochem. Commun. 8 (2006) 1588.
[84] P.E. Laibinis, J.J. Hickman, M.S. Wrighton, G.M. Whitesides, Science 245 (1989) 845.
[85] G.M. Whitesides, J.P. Mathias, C.T. Seto, Science 254 (1991) 1312.
[86] L.F. Rozsnyai, M.S. Wrighton, J. Am. Chem. Soc. 116 (1994) 5993.
[87] J.C. Love, D.B. Wolfe, M.L. Chabinyc, K.E. Paul, G.M. Whitesides, J. Am. Chem. Soc. 124 (2002) 1576.
[88] S. Sawada, Y. Masuda, P. Zhu, K. Koumoto, Langmuir 22 (2006) 332.
[89] C. Zhou, G. Nagy, A.V. Walker, J. Am. Chem. Soc. 127 (2005) 12160.
[90] K.C. Chan, T. Kim, J.K. Schoer, R.M. Crooks, J. Am. Chem. Soc. 117 (1995)5875.
[91] K.S.L. Chong, S. Sun, G.J. Leggett, Langmuir 21 (2005) 3903.